RSC Advances

REVIEW

View Article Online
View Journal | View Issue

Cite this: *RSC Adv.*, 2022, **12**, 18945

Recent developments in supramolecular complexes of azabenzenes containing one to four N atoms: synthetic strategies, structures, and magnetic properties

Juhi Singh,† Suvam Kumar Panda † and Akhilesh Kumar Singh *

Received 3rd June 2022
Accepted 20th June 2022

DOI: 10.1039/d2ra03455g

rsc.li/rsc-advances

For the last couple of decades, azabenzene-based ligands have drawn much attention from inorganic chemists due to their ability to coordinate with different metal ions to form supramolecular clusters. These azabenzenes are weak σ donors and strong π acceptors and electron-deficient. Metallogrid complexes and non-grid oligomers are well-defined supramolecular clusters, formed by appropriate chelating ligands, and can show interesting optical, magnetic, and electronic properties. Self-assembly of [$n \times n$] metallogrid complexes is dominated by the entropic factor while the formation of oligonuclear metal ion complexes is dominated by other effects like CFSE, electrostatic factors, ligand conformational characters, *etc.* Herein, the present article gives an overview of six-membered heterocyclic azine-based ligands and their potential for different metal ions to form polynuclear complexes. Moreover, their temperature-dependent magnetic properties and SCO phenomena are well described and tabulated.

1. Introduction

In heterocyclic chemistry, according to Hantzsch–Widman nomenclature, azabenzene (azine) refers to the compounds containing six-membered aromatic rings with one or more N atoms in the heterocyclic ring.[1] Heterocyclic azines are named depending on n, the number of N atoms present in the aromatic six-membered heterocyclic ring, *e.g.* $n = 1$ (pyridine); $n = 2$ (diazine: pyrimidine, pyridazine, pyrazine); $n = 3$ (1,3,5-triazine); and $n = 4$ (1,2,4,5-tetrazine). These azabenzenes form supramolecular clusters with different transition and inner-transition metal ions and show variable magnetic responses at different temperatures. The roots of modern supramolecular chemistry were first described by Hermann Emil Fischer in 1894.[2] After that in 1979, Lehn defined Supramolecular Chemistry as "chemistry beyond the molecule".[3] Supramolecular systems are held together by hydrophobic forces, π–π interactions, or electrostatic effect, *i.e.*, metals don't coordinate by direct covalent forces.[4] Molecular self-assembly is the basic concept behind Supramolecular Chemistry.[5] Synthetic

School of Basic Sciences, Indian Institute of Technology Bhubaneswar, Bhubaneswar, 752 050, India. E-mail: aksingh@iitbbs.ac.in

† These authors made equal contributions.

Juhi Singh completed her BSc (Hons.) in Chemistry from the University of Delhi in 2018. She is currently pursuing her Masters in Chemistry from Indian Institute of Technology, Bhubaneswar and working on "Magnetochemistry of [n × n] Grid Complexes".

Suvam Kumar Panda obtained his BSc (Hons.) from the Utkal University in 2015 followed by MSc from North Orissa University, Odisha. After obtaining his MSc degree in 2017, he moved to the Indian Institute of Technology, Bhubaneswar to pursue his doctoral studies, where he joined the research group of Dr A. K. Singh in 2018. Since then he has been exploring various acyclic/macrocyclic organic ligands and their complexes for magnetic and bio-imaging applications.

coordination chemists mainly focus on the preparation of polynuclear transition metal-based self-assembled multimetallic clusters because they show fascinating magnetic, electronic, redox, and photophysical properties.[6] Desired supramolecular clusters can be synthesized by an appropriate choice of bridging groups and chelating ligands. For example, $[n \times n]$ grids are formed by ligand-directed-assembly process to form polynuclear complexes, in which $2n$ number of ligands are arranged like poles of a grid with n^2 metal ions situated at the joint of the grid (Fig. 1). These types of grids are called homometallic $[n \times n]$ grids. When both n values are different then the formed self-assembly grid is called $[n \times m]$ heterometallic grid, in which all metal centres are not same. So in molecular magnetism and coordination chemistry, metallogrid complexes hold a special place due to their inventive structure and used for information storage devices, logic and electronic switches.[7] Nuclearity of grid assembly or coordination capacity of ligands can be extended by using suitable different bridging groups substituted with different functional groups at terminal ends.[8–10]

1.1 Magnetism

Magnetism in a material largely arises due to a magnetic moment that is generated by the electrons' intrinsic spin.[11] In presence of external magnetic field alignment of ground state spins of electrons show attractive or repulsive responses. This results into two kinds of magnetism, diamagnetism and paramagnetism. Diamagnetism arises due to presence of paired electron materials which show repulsive response to applied magnetic fields. Paramagnetism is shown by species having unpaired electrons and their spins align in the same direction as of applied magnetic field. They show attractive response towards applied magnetic fields (Fig. 2).

1.2 Temperature- and field-dependent magnetic properties

In a complex, paramagnetic metal centres show intramolecular magnetic coupling with each other in presence of an applied magnetic field and below a certain temperature (Curie and Néel points), alignment of neighboring spins change rapidly (Fig. 3b and c).[11,12] Alignment of spins in an antiparallel direction give rise to antiferromagnetism and alignment of spins in uniform parallel direction give rise to ferromagnetism (Fig. 2b and c). Paramagnetic substances obey Curie law *i.e.*, $\chi = C/T$, where χ is magnetic susceptibility (degree of magnetization), T is absolute temperature, and C is curie constant. But curie law was unable

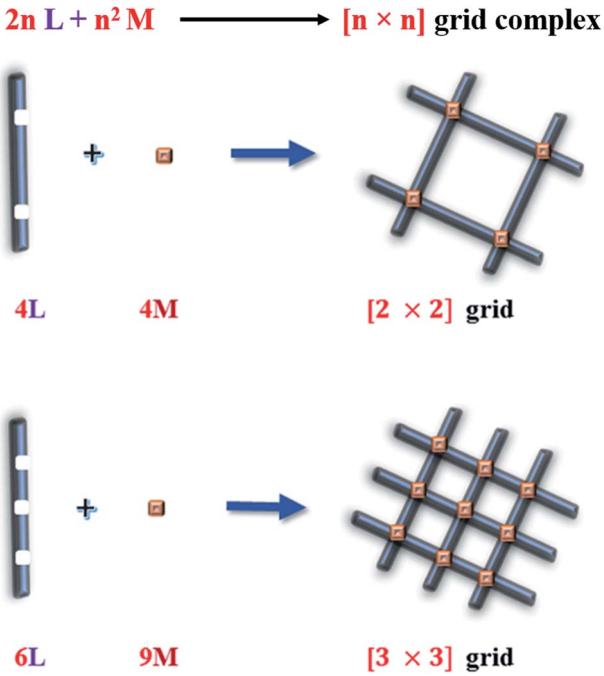

Fig. 1 Ligand directed self-assembly in metallogrid complexes.

Akhilesh Kumar Singh finished his PhD in 2007 from Indian Institute of Technology Kanpur (IIT Kanpur). He carried out his first post-doctoral research at Georg August University Goettingen, Germany followed by second post-doctoral research at Ecole Normale Superiere de Lyon, France. In 2010, he joined Indian Institute of Technology Bhubaneswar as an assistant professor. His research interests include "(1) Magnetochemistry, (2) T1, T2 and paraCEST-based Contrast Agent for MRI and (3) Fluorogenic and Chromogenic Chemosensors". Apart from these, he also works in the field of "Ionic Liquids and Their Energy Applications in Lithium-Ion Battery".

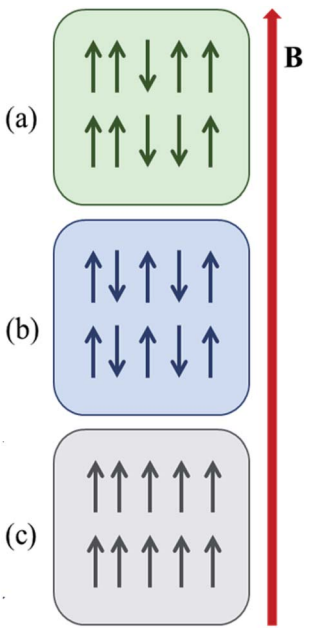

Fig. 2 Different arrangementof neighbouring spin; (a) paramagnetism, (b) antiferromagnetism, and (c) ferromagnetism.

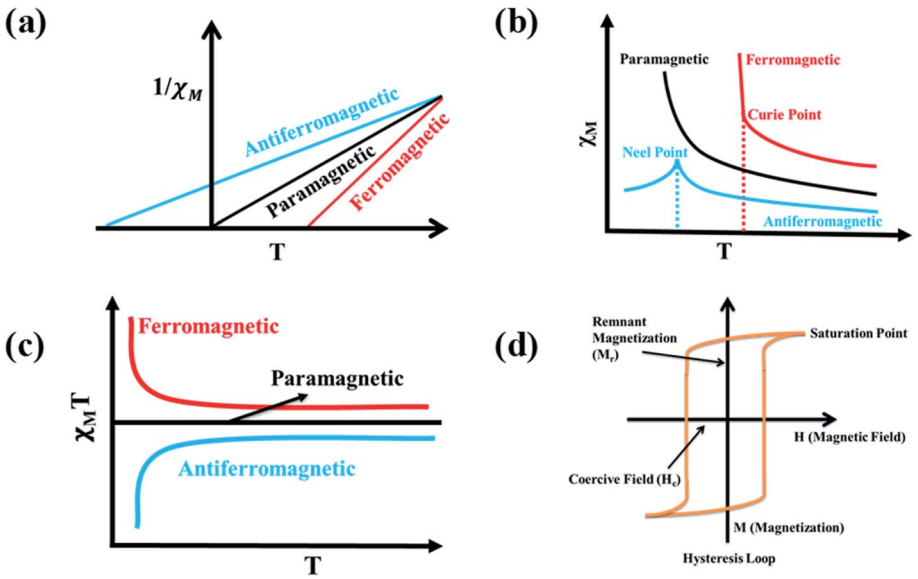

Fig. 3 Characteristic graphs of (a) $1/\chi_M$ *vs.* *T*, (b) χ_M *vs.* *T*, (c) $\chi_M T$ *vs.* *T* for paramagnetic, ferromagnetic, and antiferromagnetic substances, (d) Hysteresis loop.

to describe the behaviour of ferromagnetic and antiferromagnetic substances, so to overcome this problem Curie–Weiss law *i.e.*, $\chi = C/(T - \theta)$ came into picture where θ is the Curie Weiss constant (For ferromagnetic substances $\theta > 0$ and for antiferromagnetic substances $\theta < 0$) as shown in Fig. 3a.[13,14] Ferromagnetic substances show hysteresis behaviour and form a hysteresis loop shown in Fig. 3d. Hysteresis loops give two important terms, coercive field (H_c) and remnant magnetization (M_r). Twice of the coercive field is equal to the maximum width of the hysteresis loop and is defined as the field required demagnetizing the fully magnetized material. Remnant magnetization is defined as the magnetization that remains after removal of the applied magnetic field. Hysteresis loop is used for the characterization of soft and hard magnets (Fig. 4).

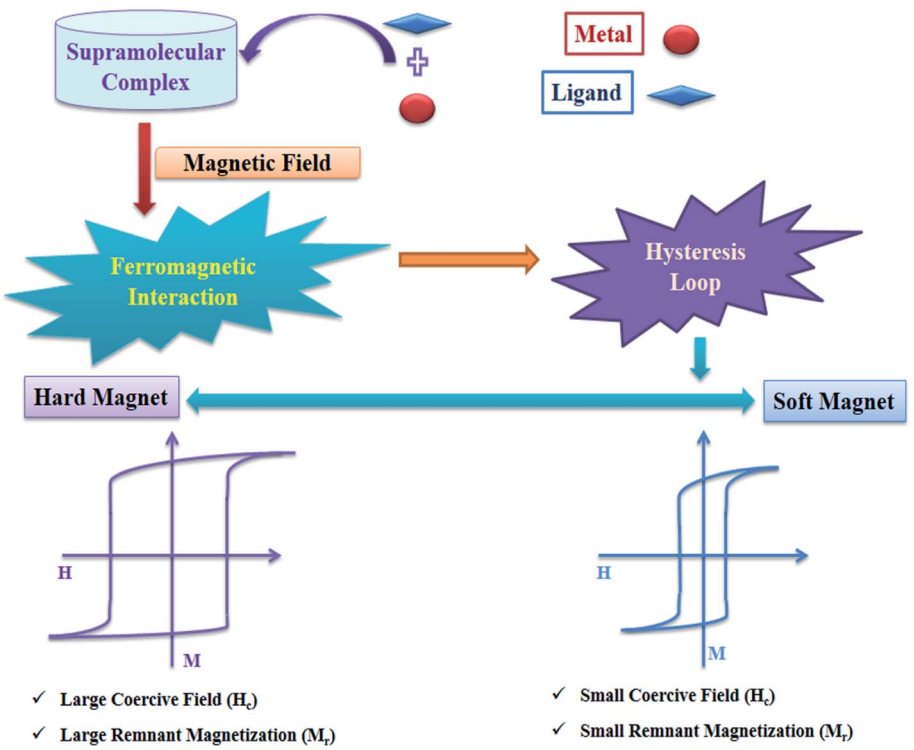

Fig. 4 Schematic representation of hysteresis loop in ferromagnetic materials.

Soft magnets have less H_c value and approximately zero value of M_r, used in magnetic shielding and electric motors. But hard magnets have higher value of H_c and significant value of M_r, used in data storage devices.[10]

1.3 Device for magnetic measurement

The common effective and sensitive device that is used for measuring the magnetic properties is SQUID (Superconducting quantum interference device) magnetometer.[15] It is made of superconductors those are separated by thin insulating layers (Josephson junction) and can detect small magnetic fields.[16] These SQUID magnetometers are now commonly used in magnetic coupling measurements between two paramagnetic centres. SQUID magnetometers normally operate at low temperature to room temperature *i.e.*, at liquid helium or liquid nitrogen temperature to room temperature and they consist of superconductors that are separated by appropriately thin insulating layers or junctions, known as Josephson junctions, through which electrons can flow.[17] When current flows through SQUID, magnetic flux (Φ) is generated by the samples inside the apparatus and the superconducting coils. When the sample is moved up and down inside the SQUID an alternating magnetic flux is generated within the pick-up coil and through a superconducting pick-up coil, the magnetic signal is obtained. The magnetic flux is transferred by this coil from the sample to a radio frequency SQUID device within the liquid helium bath and found far away from the sample. As a result, this can act as a magnetic flux-to-voltage converter device. This voltage is then amplified and gives the information regarding the materials' magnetic properties (magnetic susceptibility and effective magnetic moment).[18–20] This is used widely in research, biological studies, electronic measurements, and instruments in which conventional measurement fails to sense the faint signals.[21] Characteristic graphs shown in Fig. 3 are produced by the data obtained from a SQUID magnetometer.

1.4 Magnetic interaction

There are the two categories of magnetic materials: (a) magnetically concentrated and (b) magnetically dilute substances. In magnetically dilute substances, due to a large distance of separation between individual paramagnetic centres, interaction between them is not possible.[22] On the other hand, in magnetically concentrated substances direct exchange or superexchange interaction occurs between total-electron-spin of paramagnetic centres, which is clearly due to the small inter-micromagnetic separation.[23] In the direct-exchange, there is an interaction between two nearby cations without involving any intermediate anion; while superexchange refers to a strong magnetic exchange interaction, which involves the coupling between nearby cations through a non-magnetic anion.[24,25]

In metallogrid complexes, spin exchange interaction takes place between the paramagnetic metal centers through the diamagnetic bridging groups. So, to determine the interactions among all spin centers, ligand field effects, and Zeeman splitting terms, a generalized spin Hamiltonian equation can be used for the evaluation of multimetallic cluster assemblies.[26,27]

$$H = -\sum_{i<j} J_{ij} S_i S_j + \sum_i S_i D_i S_i + \mu_B \sum_i S_i g_i B \quad (1)$$

where D = zero field splitting.

Normally, in isotropic and spin only conditions the ligand field effects, $\sum_i S_i D_i S_i$, are ignored and by assuming the Lande splitting factor (g) are identical and isotropic for all spin centres, the Hamiltonian can be written as

$$H = -\sum_{i<j} J_{ij} S_i S_j \quad (2)$$

When the Hamiltonian applied on a specific spin-coupled arrangement, it provides a square matrix and on diagonalization it provides the energy of the subsequent spin states (S') in form of S_i, S_j and J.

$$E(S') = -J(S'(S' + 1) - S_i(S_i + 1) - S_j(S_j + 1) \quad (3)$$

where, S' is permitted to take the values $S_i + S_i$, $S_i + S_j - 1$, …, $S_i - S_j$.

When $J > 0$ (Ferromagnetic Substances), $(S_i + S_j)$ is the spin states for ground state and $(S_i - S_j)$ is the spin states for excited state and *vice versa* for $J < 0$ (antiferromagnetic substances).

Based on the resultant spin Hamiltonian, estimation of the magnetic behaviour of metallogrid complexes can be executed for isotropic exchange interaction.[28] This can be generalized by Heisenberg-Dirac-Van-Vleck (HDVV) equation:

$$\chi_m = \frac{N\beta^2 g^2}{3k(T-\theta)} \frac{\sum S'(S'+1)(2S'+1)e^{-E(S')/kT}}{\sum(2S'+1)e^{-E(S')/kT}}(1-\rho)$$

$$\frac{N\beta^2 g^2 S(S+1)\rho}{3kT} + \mathrm{TIP} \quad (4)$$

where, $E(S')$ = Energy of the exchange-coupled spin states, ρ = mole fraction of paramagnetic impurity, TIP = temperature independent paramagnetism, arises due to the mixing of the excited state and ground state in presence of external applied magnetic field, and θ = Weiss-like temperature correction.

In this review, azabenzene-based ligands such as pyridine, pyridazine, pyrimidine, pyrazine, 1,3,5-triazine, 1,2,4,5-tetrazine and their derivatives are highlighted under the umbrella termed as azabenzene. These azabenzene containing compounds are used to prepare a variety of polytopic ligands which upon metalation lead to the formation of grid complexes. The iron and cobalt complexes of these ligands show interesting magnetic properties and sometimes spin crossover (SCO) phenomena as well. SCO materials show crossover between the low spin and high spin states and they may be used in data storage,[29,30] molecular switches,[31] and optical displays.[32] Generally, in octahedral d^4–d^7 transition metal complexes, the transition between LS and HS is observed due to the presence of intermediate ligand field and the variation of temperature, pressure, or light.[33] There are a few reports of grid complexes of azabenzene-based ligands which show ferromagnetic

Table 1 Summary of the discussed complexes and their magnetic responses used in the current review[a]

S.No.	Ligands	Compound	Magnetic order	Grid	Ref.
1	L1	$[((L1)_2Dy_4)(\mu_2\text{-}O)_4]\text{-}(H_2O)_8\cdot 2CH_3OH\cdot 8H_2O$	A.F.M.	—	43
		$[((L1)_2Ho_4)(\mu_2\text{-}O)_4]\text{-}(H_2O)_8\cdot 6CH_3OH\cdot 4H_2O$	A.F.M.	—	
2	L2	$[Dy_4(L2)_4(\mu_2\text{-}OH)_3(\mu_2\text{-}OMe)]_4NO_3\cdot 2MeOH\cdot 4H_2O$	A.F.M.	[2 × 2]	44
		$[Tb_4(L2)_4(\mu_2\text{-}OH)_3(\mu_2\text{-}OMe)]_4NO_3\cdot 2MeOH\cdot 4H_2O$	A.F.M.	[2 × 2]	
		$[Gd_4(L2)_4(\mu_2\text{-}OH)_3(\mu_2\text{-}OMe)]_4NO_3\cdot 2MeOH\cdot 5H_2O$	A.F.M.	[2 × 2]	
		$[Er_4(L2)_4(\mu_2\text{-}OH)_3(\mu_2\text{-}OMe)]_4NO_3\cdot 3MeOH\cdot 3H_2O$	A.F.M.	[2 × 2]	
3	L3	$[Cu_{16}(L3)_8](dmf)_3$	A.F.M.	[4 × 4]	45
4	L4	$[Dy_4(L4)_4(H_2O)_{12}](CF_3SO_3)_4\cdot 12H_2O$	A.F.M.	[2 × 2]	46
		$[Dy_4(L4')_4Cl_4(H_2O)_8]Cl_8$	A.F.M.	[2 × 2]	
5	L5	$[Dy_4Cu_4(L5)_4Cl_8(H_2O)_4]Cl_4\cdot 28H_2O$	F.M.	[2 × 2]	46
6	L6	$[Dy_4(L6_2)_4(\mu_2\text{-}OH)_4]\cdot x CH_3OH\cdot yH_2O$	A.F.M.	[2 × 2]	51
		$[Tb_4(L6_2)_4(\mu_2\text{-}OH)_4]\cdot x CH_3OH\cdot yH_2O$	A.F.M.	[2 × 2]	
		$[Ho_4(L6_2)_4(\mu_2\text{-}OH)_4]\cdot x CH_3OH\cdot yH_2O$	A.F.M.	[2 × 2]	
		$[Er_4(L6_2)_4(\mu_2\text{-}OH)_4]\cdot x CH_3OH\cdot yH_2O$	A.F.M.	[2 × 2]	
7	L7	$[Mn_{10}(L7')_6(H_2O)_5][Mn(H_2O)_6]_2\cdot 11H_2O$	A.F.M.	[3 × 3]	10
8	L8	$[Mn_{11}(L8')_6(H_2O)_8][Mn(H_2O)_6]\cdot 24H_2O$	A.F.M.	[3 × 3]	10
9	L9	$[Fe^{III}{}_4(L9')_4]$	A.F.M.	[2 × 2]]	52
		$[Fe^{II}{}_2Fe^{III}{}_2(L9)_4](BF_4)_2\cdot 2CH_3CN$	A.F.M.	[2 × 2]	
		$[Mn_4(L9)_4]\cdot MeCN$	A.F.M.	[2 × 2]	
		$[Co_4(L9)_4]\cdot CHCl_3$	A.F.M.	[2 × 2]	
		$[Cu_4(L9)_4]\cdot CHCl_3$	A.F.M.	[2 × 2]	
10	L10	$[Dy(L10)(H_2O)](ClO_4)\cdot 2CH_3CH_2OH$	A.F.M.	—	53
		$[Dy(L10)(NO_3)]$	A.F.M.	—	
		$[Dy_2(L10)(dbm)_4]$	F.M.	—	
11	L11	[Dy(L11)Cl]	—	—	54
		[Dy(L11)Br]	—	—	
12	L12	$[Cu_2(L12)_2]$	D.M	—	55
		$[Ni_2(L12)_2]$	A.F.M.	—	
13	L13	$[Fe^{II}(L13)](ClO_4)_2\cdot H_2O$	S.C.O	—	56
		$[Co^{II}(L13)](ClO_4)_2\cdot H_2O$	—	—	
		$[Fe_{0.4}Co_{0.6}{}^{II}(L13)](ClO_4)_2\cdot H_2O$	S.C.O	—	
14	L14	$[Cu(L14)_2(ClO_4)]ClO_4$	A.F.M.	—	73, 74 ,[76] and 77
		$[Cu_2(L14)(OH)\text{-}(ClO_4)_3(H_2O)_3].H_2O$	A.F.M.	—	
		$[Cu_2(L14)_2(H_2O)_2](ClO_4)_4$	A.F.M.	—	
		$[Cu_2(L14)_2(ClO_4)_4]$	A.F.M.	—	
		$[Cu_2(L14)(N_3)_4].H_2O/[Cu_2(L14)\text{-}(N_3)_4(H_2O)])_n$	A.F.M.	—	
		$[Cu_2(L14)(OH)(dca)_3]\cdot H_2O)_n$	A.F.M.	—	
		$[Ni_4(L14)_4(\mu\text{-}N_3)_4]Cl_4\cdot 5H_2O$	F.M.	[2 × 2]	
		$[Co^{II}{}_4(L14)_4(N_3)_4])\cdot sol$	F.M. and A.F.M	[2 × 2]	
		$[Fe^{II}{}_4\ (L14)_4\ (N_3)_4][BPh_4]_4\cdot sol$	S.C.O	[2 × 2]	
15	L15	$[(L15)_4\ Co^{II}{}_4(N_3)_4]\cdot sol$	F.M. and A.F.M.	[2 × 2]	76 and 77
		$[(L15)_4Fe^{II}{}_4\ (N_3)_4][BPh_4]_4\cdot sol$	A.F.M	[2 × 2]	
16	L16	$[Dy_4(HL16)_2L(DMF)_8]\cdot 2ClO_4CH_2Cl_2\cdot 4DMF(CH_3CH_2)_2O\cdot H_2O$	F.M.	—	78
		$[Dy_6\ (L16)_3(PhCOO)_6(CH_3OH)_6]\cdot 11CH_3OH\cdot H_2O$	A.F.M.	—	
		$[Dy_{10}Na_2\ (L16)_4(\mu_3\text{-}OH)_4(DMF)_{12}\text{-}(NO_3)_6]\cdot 6NO_3\cdot 2DMF(CH_3CH_2)_2O\cdot H_2O$	A.F.M.	—	
17	L17	$Fe_2L17(H_2O)_4(BF_4)_4$	A.F.M.	—	91
		$Co_2L17(H_2O)_3(MeCN)_2(BF_4)_4$	A.F.M.	—	
		$Ni_2L17(H_2O)_4(BF_4)_4$	A.F.M.	—	
		$Fe_4(L17)_2(F)_4(BF_4)_4\cdot 52H_2O$	A.F.M.	—	
		$Co_4(L17)_2(F)_4(BF_4)_4\cdot 3H_2O$	A.F.M.	—	
		$Ni_4(L17)_2(F)_4(BF_4)_4\cdot 4H_2O$	A.F.M.	—	
18	L18	$[Fe_4(HL18a)_4]Cl_4\cdot 9H_2O$	S.C.O	[2 × 2]	92 and 93
		$[Fe_4(L184a)_2(H_2L18a)_2]\cdot(BF_4)_4\cdot 6H_2O$	S.C.O	[2 × 2]	
		$[Fe_4(L18b)_2(H_2L18b)_2]ClO_4)_4\cdot 4H_2O$	D.M.	[2 × 2]	
		$[Co_4(HL18a)_4](ClO_4)_4\cdot 8H_2O$	S.C.O	[2 × 2]	
		$[Co_4(L18b)_4](ClO_4)_4\cdot 16H_2O$	D.M	[2 × 2]	
19	L19	$[Fe_4(L19)_4](BF_4)_8\cdot x MeCN$	S.C.O.	[2 × 2]	94
		$[Fe_4(H_2L19)_2(HL19)_2](BF_4)_6\cdot 8MeCN$	S.C.O.	[2 × 2]	
		$[Fe_4(HL19)_4](BF_4)_4\cdot 12MeCN$	S.C.O.	[2 × 2]	
		$[Zn_4(H_nL19_4)]^{(n)+}$ $(n = 8$ and $4)$	D.M.	[2 × 2]	
20	L20	$[Ni_4(L20)_4].2CH_3CN\cdot 4CH_3OH\cdot 4H_2O$	A.F.M.	[2 × 2]	95
21	L21	$[Ni_4(H_2L21)_4](CF_3SO_3)_8\cdot 4CH_3NO_2\cdot 8H_2O$	A.F.M.	[2 × 2]	95
22	L22	$[Dy_4(L22)_4(H_2O)_4(NO_3)_4]\cdot 6CH_3OH\cdot 6H_2O$	A.F.M.	[2 × 2]	99

Table 1 (*Contd.*)

S.No.	Ligands	Compound	Magnetic order	Grid	Ref.
23	L23	$[Co_4(L23^{H})_4](ClO_4)_4 \cdot 6DMF \cdot 3H_2O$	D.M.	—	104
		$[Co_4(L23^{Me})_4](ClO_4)_8 \cdot 4MeCN \cdot H_2O$	S.C.O.	—	
		$[Co_4(L23^{Br})_4](ClO_4)_8 \cdot CH_3OH \cdot 2MeCN \cdot 5H_2O$	A.F.M.	—	
24	L24	$[Zn_3(L24)_3](BF_4)_6$	—	—	100
		$[Fe_3(L24)_3](BF_4)_6$	—	—	
25	L25	$((H_2O)Mn^{II}L25)(\mu\text{-}1,3\text{-}N_3)(L21Mn^{II}(NO_3))](NO_3)_2$	A.F.M.	—	110
		$[(L25Mn^{II})(\mu\text{-}1,3\text{-}N_3)]_n(NO_3)_n$	A.F.M.	—	
26	L26	$[Cu_4(L22)_4]^{8+}$	F.M.	[2 × 2]	111
27	L27	$[Fe(L27^{H})_2(NCS)_2] \cdot 2CH_2Cl_2$	S.C.O.	—	33
		$[Fe(L27^{F})_2(NCS)_2] \cdot 2CH_2Cl_2$	S.C.O.	—	
28	L28	$[Dy_4(L28)_2(CH_3OH)_3(NO_3)_3] \cdot 3NO_3 \cdot 2H_2O$	A.F.M.	—	122
		$[Dy_4(L28)_2(CH_3OH)_2(SCN)_4(OCH_3)_2] \cdot 2CH_3OH \cdot 2H_2O$	A.F.M.	—	
		$([Dy_4(L28)_2(CH_3OH)(SCN)_6(CH_3CN)] \cdot 3CH_3OH \cdot 4CH_3CN)_2$	A.F.M.	—	
		$[Dy_4(L28)_2(CH_3OH)_2(SCN)_6] \cdot 6CH_3OH \cdot 2H_2O$	A.F.M.	—	
		$[Dy_4(L28)_2(CH_3OH)_2(SCN)_4(OCH_3)_2] \cdot 5CH_3OH \cdot 2H_2O$	A.F.M.	—	
		$[Dy_4(L28)_2(CH_3OH)(SCN)_5(H_2O)_2] \cdot SCN \cdot 4CH_3OH \cdot 2H_2O$	A.F.M.	—	
29	L29	$[Dy(tmhd)_3]_2(L29)$	A.F.M.	—	133
		$(Cp_2Co)([Dy(tmhd)_3]_2(L29))$	A.F.M.	—	
		$[Co_4(L29)_4(dbm)_4] \cdot 4MeCN$	A.F.M.	[2 × 2]	
30	L30	$[Dy_4(L30)_4(MeOH)_8](NO_3)_4 \cdot a MeOH \cdot b H_2O$	F.M.	—	135
		$[Gd_4(L30)_4(MeOH)_8](NO_3)_4 \cdot aMeOH \cdot bH_2O$	F.M.	—	
31	L31	$[Ni_4(L26)Cl_6(DMF)_8]Cl \cdot 1/2(H_2O)$	F.M.	—	136
32	L32	$[Dy^{III}_2(L28)(THMD)_6] \cdot 4(C_6H_6)$	A.F.M.	—	139
		$[Dy^{III}_2(L28)_2)(THMD)_4]$	A.F.M.	—	

[a] A.F.M. = antiferromagnetic, F.M. = ferromagnetic, D.M. = diamagnetic, S.C.O. = spin crossover.

interaction and form hysteresis loop at particular temperature. Some of these ligands and their magnetic behaviours are described below based on the recent articles. Finally, all the results are highlighted in a tabular manner for the better understanding of the readers (Table 1).

1.5 Rationale for choosing such azabenzene-based ligands

Polytopic pyridine/pyrimidine/pyrazine/pyridazine/triazine/tetrazine and hydrazone-based ligands depict the power of self-assembly as a methodology for the synthesis of polymetallic systems with specific and predetermined organization of metal centers in a closely spaced bridged arrangement. Homometallic, heterometallic, homovalent, heterovalent and mixed-spin-state $[n \times n]$ $(n \geq 2)$ square-grids, $[n \times m]$ $(n, m \geq 2)$ rectangular-grids or non-grid oligomeric structures may be isolated using these ligands to give an interesting structural and magnetic properties. These ligands have potential to provide the supramolecular assembly with interesting magnetic properties having ferromagnetic, antiferromagnetic and ferrimagnetic interactions between the metal centers. The magnetic properties of such supramolecular assembly may be exploited for molecular devices, molecular switches[31] and for information storage and processing devices.[29,30]

2. Pyridine-based ligands

Pyridine is a six-membered N-heterocyclic compound, discovered by Scottish chemist Thomas Anderson in 1849.[34,35] Pyridine is able to form σ bond with metal centre by overlapping the sp^2 lone pair orbital of N atom with vacant metal orbitals. Due to this reason pyridine can be utilized as a ligand for the development of metal complexes. Pyridine and its derivatives are widely used in coordination chemistry. Inorganic chemists take very much interest in design and synthesis of polytopic pyridine hydrazone-based ligands. These polytopic pyridine-based ligands are widely utilized in self-assembled $[n \times n]$ and $[n \times m]$ grid complex formations.[36–42] Some of these ligands, based on the recent literature, which have potential towards self-assembly for the syntheses of polymetallic complexes are described in this current review (Scheme 1).

In 2013 Chandrasekhar *et al.* reported the ligand **L1**, which formed a tetranuclear complexes $[((\mathbf{L1})_2Dy_4)(\mu_2\text{-}O)_4]\text{-}(H_2O)_8 \cdot 2CH_3OH \cdot 8H_2O$ (**DyL1**) and $[((\mathbf{L1})_2Ho_4)(\mu_2\text{-}O)_4] \cdot (H_2O)_8 \cdot 6CH_3OH \cdot 4H_2O$ (**HoL1**) with lanthanide salts $LnCl_3 \cdot 6H_2O$ (Ln = Dy^{III} or Ho^{III}).[43] In tetranuclear complexes, all lanthanide ions were situated in the plane and held together by perpendicularly arranged deprotonated ligands, which were coordinated *via* their two coordination pockets ONO and ONNO. All these arrangements formed tetranuclear complexes that showed temperature-dependent magnetic susceptibility between 2 and 300 K. Initially, the $\chi_m T$ values were found as 53.4 $cm^3\ mol^{-1}$ K for complex **DyL1** and 53.0 $cm^3\ mol^{-1}$ K for complex **HoL1**, that slowly decreased as the temperature was lowered and suddenly at below 30 K the $\chi_m T$ values were steeply decreased and reached to 29.6 and 21.0 $cm^3\ mol^{-1}$ K at 2 K for **DyL1** and **HoL1**

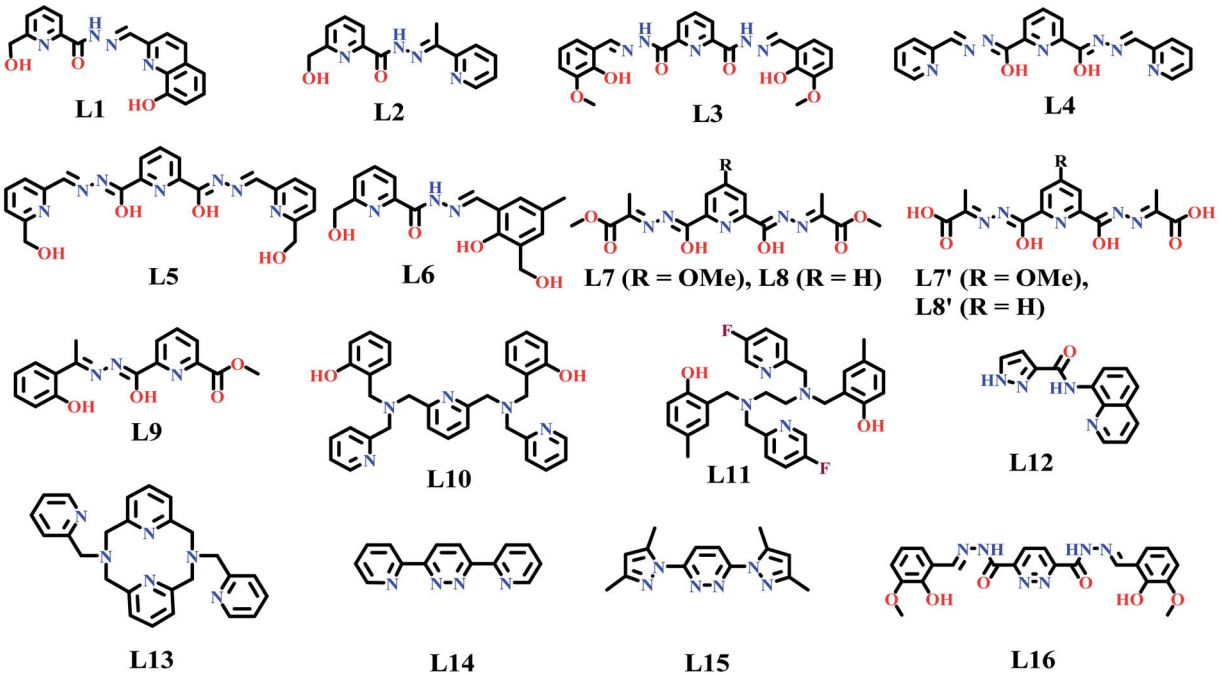

Scheme 1 Pyridine and pyridazine based ligands discussed in the present review.

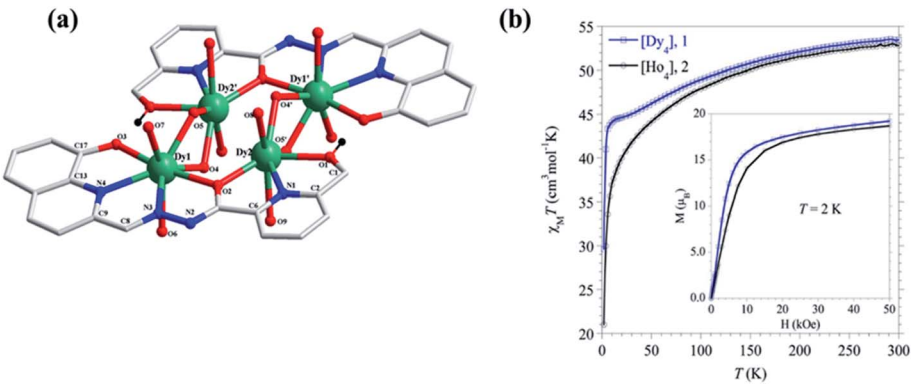

Fig. 5 (a) represents structure of complex **DyL1** and (b) show magnetic behaviour of complex **DyL1** (blue) and **HoL1** (black). Reproduced with permission from ref. 43 Copyright© 2013, American Chemical Society.

respectively. These behaviours of complexes suggested the antiferromagnetic coupling among metal centres (Fig. 5).

Again to explore more toward lanthanide complexes, in 2014, the same group reported the ligand **L2**, which formed tetranuclear [2 × 2] homometallic grid complexes, $[Ln_4(\mathbf{L2})_4(\mu_2\text{-}OH)_3(\mu_2\text{-}OMe)]_4NO_3 \cdot x\text{MeOH} \cdot y\text{H}_2\text{O}$ (Ln = Dy, Tb, Gd, and Er), when reaction was done with different hydrated lanthanide(III) salts $Ln(NO_3)_3\ x\text{H}_2\text{O}$ (Ln = Dy, Tb, Gd, and Er).[44] The ligand backbone contained two unsymmetrical coordination pockets (NNO & ONO) and was able to connect with two lanthanide ions. So, in **DyL2**, **TbL2**, **GdL2** and **ErL2** lanthanide centres were eight coordinated and satisfied by NNO and ONO coordination pockets of perpendicular ligands and additional two coordinations were fulfilled by μ-OH and μ-OMe ligands. So overall, in grid complexes two Ln^{III} ions were coordinated with 6O, 2N and the remaining two Ln^{III} ions contained coordination environments of 4O, 4N. For analyzing the magnetic property of **GdL2**, magnetic susceptibility measurement was done. Initially at 290 K, the $\chi_m T$ value was 30.9 $cm^3\ mol^{-1}$ K, that continuously decreased on lowering the temperature, indicated the dominating nature of antiferromagnetic interactions among the Gd^{III}-centers. Same type of behaviour was shown by other lanthanide complexes *i.e.*, at 290 K, $\chi_m T$ values were observed as 55.0 (**DyL2**), 46.6 (**TbL2**) and 44.1 (**ErL2**) $cm^3\ mol^{-1}$ K, that decreased down on lowering the temperature (Fig. 6).

Amit Adhikary and coworkers in 2014 reported the potential ligand **L3**, which had the inclusion of pyridine ring at the center with two *o*-vanillin groups present at the terminal and both the groups were connected by a carbohydrazide linkage.[45] At room temperature when **L3** was reacted with methanolic solution of

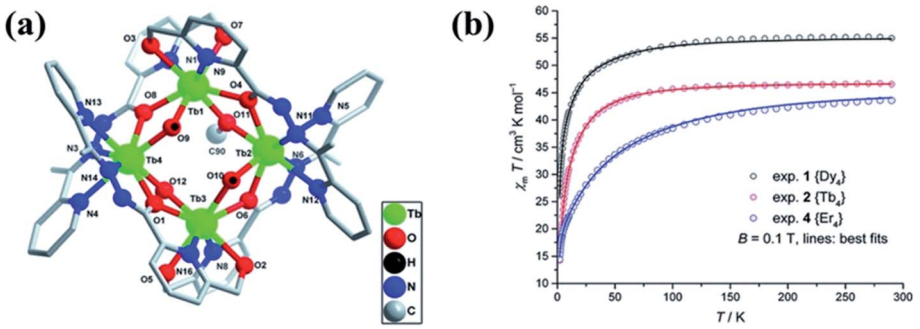

Fig. 6 (a) represents structure of TbL2 and (b) show magnetic behaviour of complex DyL2 (black), TbL2 (red), and ErL2 (blue). Modified and reproduced with permission from ref. 44 Copyright© 2014, American Chemical Society.

$Cu(ClO_4)_2 \cdot 6H_2O$ a novel [4 × 4] metallogrid complex $[Cu_{16}(\text{-}L3)_8](dmf)_3$ (**CuL3**) was formed through self-assembly. The ligand backbone contained four coordination pockets having unsymmetrical coordination modes due to the non-participation of one methoxy group present at terminal side of the ligand. The destabilization factor arisen due to the *o*-vanillin groups was greater than the stabilization factor between aromatic rings and to avoid the stearic interaction between *o*-vanillin groups in grid structure ligands were arranged in parallel manner to each other and not in eclipsed form. In **CuL3**, 8 Cu^{II} had distorted square-pyramidal geometry which was stabilized by N_1O_4 coordination pockets (two hydroxyl O atoms, one methoxy O atoms from *o*-vanillin moieties and one N atom from the hydrazone moiety) and remaining 8 Cu^{II} had distorted octahedral geometry, stabilized by N_2O_4 coordination pockets (one N atom from hydrazone moiety and one from pyridine ring, and four O atoms from the pyridine hydrazone moieties). The [4 × 4] grid structure contained nine [2 × 2] square fragment in which the central fragment was unique. The molecule had one inversion centre and fourfold rotational axis. Variable temperature magnetic susceptibility in the form of $\chi_m T$ was studied for the complex **CuL3**. Initially (at room temperature) $\chi_m T$ value of the complex was 6.43 cm^3 mol^{-1} K, which was steadily decreased down to 1.80 cm^3 mol^{-1} K when the temperature was slowly decreased to 20 K and finally at 1.8 K the value of $\chi_m T$ was decreased rapidly to 1.01 cm^3 mol^{-1} K. So, it was confirmed that, in the lower range of temperature, **CuL3** showed antiferromagnetic interaction.

To explore the susceptibility response toward heterometallic complexes, Jianfeng Wu and coworkers, in 2015, developed 4f based heterometallic grid-like complexes based on the ligand **L4**.[46] To satisfy higher coordination number of 4f based heterometallic grid, additional ligands *viz.* NO_3^-, OH^- and OAc^- also contribute in the formation of grid complexes.[47–50] A [2 × 2] metallogrid complex was formed by the reaction of ligand **L4** with $Dy(CF_3SO_3)_3 \cdot 6H_2O$ or $DyCl_3 \cdot 6H_2O$. In [2 × 2] grid complex,

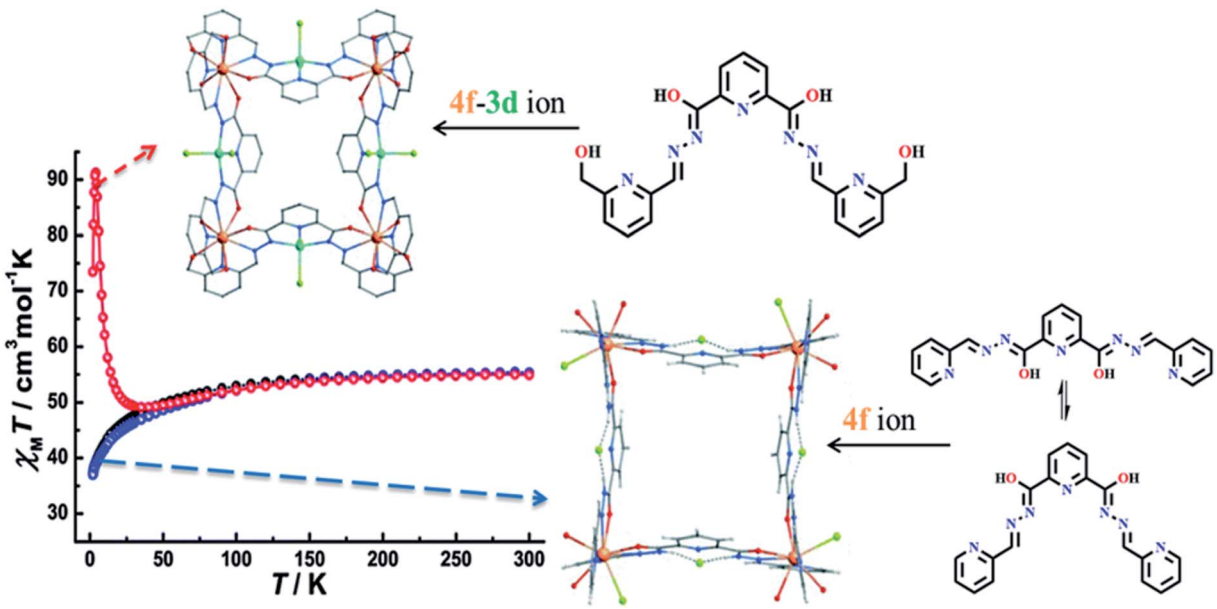

Fig. 7 Structures (orange, azure, green, blue, dark and red spheres representing Dy, Cu, Cl, N, C and O) and Magnetic properties of 4f ion (**DyL4**[b]) and 4f–3d ion (**DyCuL5**) based complexes. Modified and reproduced by permission from ref. 46, ©2015, The Royal Society of Chemistry.

all four Dy^{III} ions were joined together through four perpendicular ligands that occupied the corner sites by using terminal N–N–O pockets (Fig. 7). Here one interesting thing was observed that, after the formation of [2 × 2] 4f grid complex, there was also a possibility to form [3 × 3] or [2 × 2] 3d–4f grid complex by using free N–N–N coordination pockets of the ligand. Nevertheless, it was observed that only 4f based grid complex was formed when its further reaction was carried out with 3d and 4f metal ions. So, ligand **L4** was modified to a novel ligand **L5** with two large O–N–N–O pockets, present in terminal side, instead of two small N–N–O pockets. This made the ligand **L5** suitable for coordination with 4f metal ions and the free N–N–N pockets could bind with 3d metal ions. Heterometallic [2 × 2] grid complex $[Dy^{III}_4Cu^{II}_4\mathbf{L5}]$, was formed by the reaction of $DyCl_3\cdot 6H_2O$ and $CuCl_2\cdot 2H_2O$ with ligand **L5**, in which four Dy^{III} placed at the corner site, coordinated through the O–N–N–O pockets of ligand and one coordination sites of Dy^{III} was occupied by H_2O molecule. Four Cu^{II} ions were coordinated with the middle N–N–N pocket of ligand and two coordination sites were occupied by Cl^- ion. At room temperature χ_mT value for 4f grid-like complexes $[Dy_4(\mathbf{L4})_4(H_2O)_{12}](CF_3SO_3)_4\cdot 12H_2O$ (**DyL4**[a]) was 55.17 cm^3 K mol^{-1}, and $[Dy_4(\mathbf{L4})_4Cl_4(H_2O)_8]Cl_8$ (**DyL4**[b]) was 55.29 cm^3 mol^{-1} K that gradually decreased at 2 K to 37.4 cm^3 mol^{-1} K and 37.0 cm^3 K mol^{-1} respectively, suggested the antiferromagnetic interaction between metal centers. But in 3d–4f heterometallic grid complex, $[Dy_4Cu_4(\mathbf{L5})_4Cl_8(H_2O)_4]Cl_4\cdot 28H_2O$ (**DyCuL5**), χ_mT value first slowly decreased from 54.9 cm^3 K mol^{-1} and then sharply increased to 91.2 cm^3 K mol^{-1} at 30 K, suggested the ferromagnetic interaction and again decreased at 2 K to a minimum value of 73.5 cm^3 K mol^{-1} suggested the weak antiferromagnetic interaction Fig. 7.

In 2016 Biswas *et al.* designed and synthesized one multidentate flexible ligand **L6** which upon reaction with $Ln(NO_3)_3\cdot 5H_2O$ formed tetranuclear [2 × 2] homometallic grid complexes, $[Ln^{III}_4(\mathbf{L6}_2)_4(\mu_2\text{-}OH)_4]\cdot x CH_3OH\cdot y H_2O$ (Ln = Dy, Tb, Ho, Er), with lanthanide metals.[51] Reported ligand **L6** contained two ONO coordination pockets and was able to bind with two Ln^{III} ions. Lanthanide complexes of ligands composed of four Ln^{III} ions were held together by two coordination pockets of perpendicular dianionic ligands $[LH_2]^{2-}$. In χ_mT *vs.* T plot of **DyL6**, it was observed that the χ_mT value was 56.0 cm^3 mol^{-1} K at 300 K which further decreased to 43.9 cm^3 K mol^{-1} on lowering down the temperature to 2 K. It was also reported that similar types of magnetic behaviour were shown by the remaining three complexes.

Lakma *et al.* in 2016 reported [3 × 3] metallogrid complexes with the ligands **L7** and **L8**.[10] Both ligands were hydrolysed when the metalation was carried out with $Mn^{II}(OAc)_2\cdot 4H_2O$ and

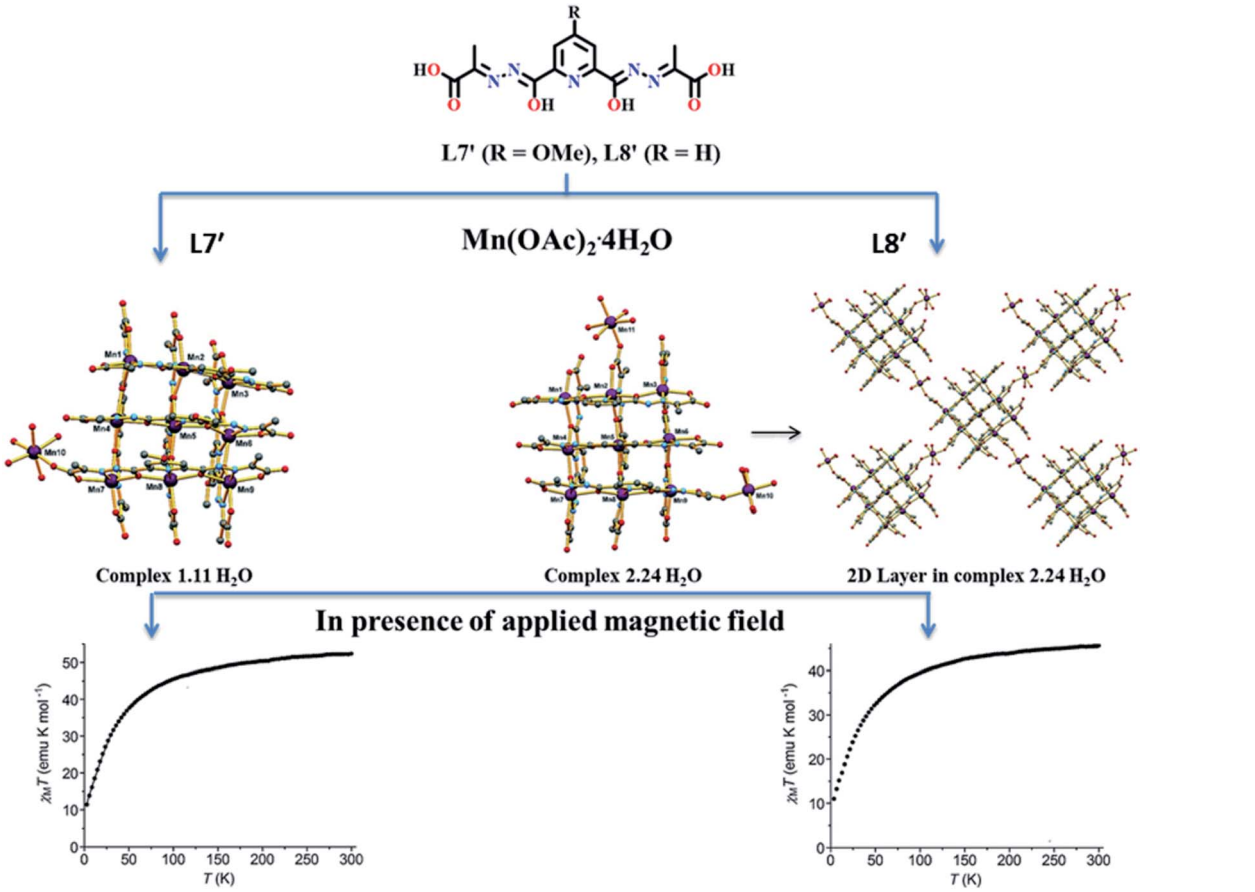

Fig. 8 Ligand L7′ and L8′ and their corresponding core structures, 1.11 H_2O and 2.24 H_2O, with their magnetic properties. Modified and reproduced by permission from ref. 10, ©2016 WILEY-VCH Verlag GmbH & Co. KGaA, Weinheim.

formed self-assembled [3 × 3] homometallic grids that contained fully deprotonated form of **L7′** and **L8′**.[10] Due to combined effect of steric and electronic factors [3 × 3] grid structure of **L7′** *i.e.*, substituted with OCH_3 group at para position organized into a 2D polymeric structure when para position was substituted with H. Pseudo-octahedral pentaaquamanganese(II) complex was formed by $[Mn_{10}(\mathbf{L7'})_6(H_2O)_5][Mn(H_2O)_6]_2\cdot 11H_2O$ ($1.11H_2O$) (Fig. 8). In the lattice of $1.11\ H_2O$, two additional $[Mn(H_2O)_6]^{2+}$ complexes were present while in $[Mn_{11}(\mathbf{L8'})_6(H_2O)_8][Mn(H_2O)_6]\cdot 24H_2O$ ($2.24H_2O$) two tetraaquamanganese(II) units were present to link between neighboring grids. In the temperature range of 300 K to 3 K, the χ_mT value of $1.11H_2O$ decreased from 52.3 to 11.4 emu K mol^{-1}, further curve was extrapolated to 9.0 emu K mol^{-1}. This nature of plot showed the antiferromagnetic interaction between metal centers. Same type of behaviour was observed for $2.24H_2O$, in which χ_mT value decreased from 45.6 emu K mol^{-1} (at 300 K) to 10.3 emu K mol^{-1} (at 3 K) and then extrapolated up to 8.7 emu K mol^{-1}.

Hossain *et al.* in 2017 reported an unsymmetrical ditopic ligand **L9**, formed tetranuclear homo valent Fe^{III} and mixed valent Fe^{II}/Fe^{III} [2 × 2] grid complex.[52] Complexes $[Fe^{III}_4(\mathbf{L9'})_4]$ (**FeL9**) and $[Fe^{II}_2Fe^{III}_2(\mathbf{L9})_4](BF_4)_2\cdot 2CH_3CN$ (**FeL9**[a]) were synthesized by using the same ligand **L9** by changing the reaction condition (Scheme 2). Mixed valent complex was formed under inert condition in which all Fe^{III}_2 Fe^{II}_2 centres were organized in a 'head-to-head' fashion while homo valent complex was formed in open air in which all Fe^{III}_4 centres were organized in 'head-to-tail' fashion. Both complexes showed response in magnetic field, at room temperature the χ_mT value for **FeL9** and **FeL9**[a] were found as 11.89 and 12.88 $cm^3\ mol^{-1}$ K respectively which upon cooling. At 2 K, the χ_mT value for **FeL9**

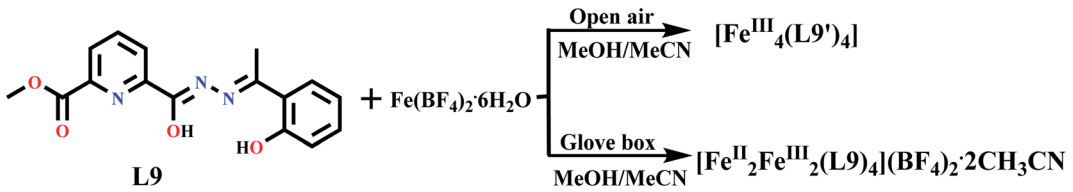

Scheme 2 Formation of **FeL9** and **FeL9**[a] under different conditions.[52]

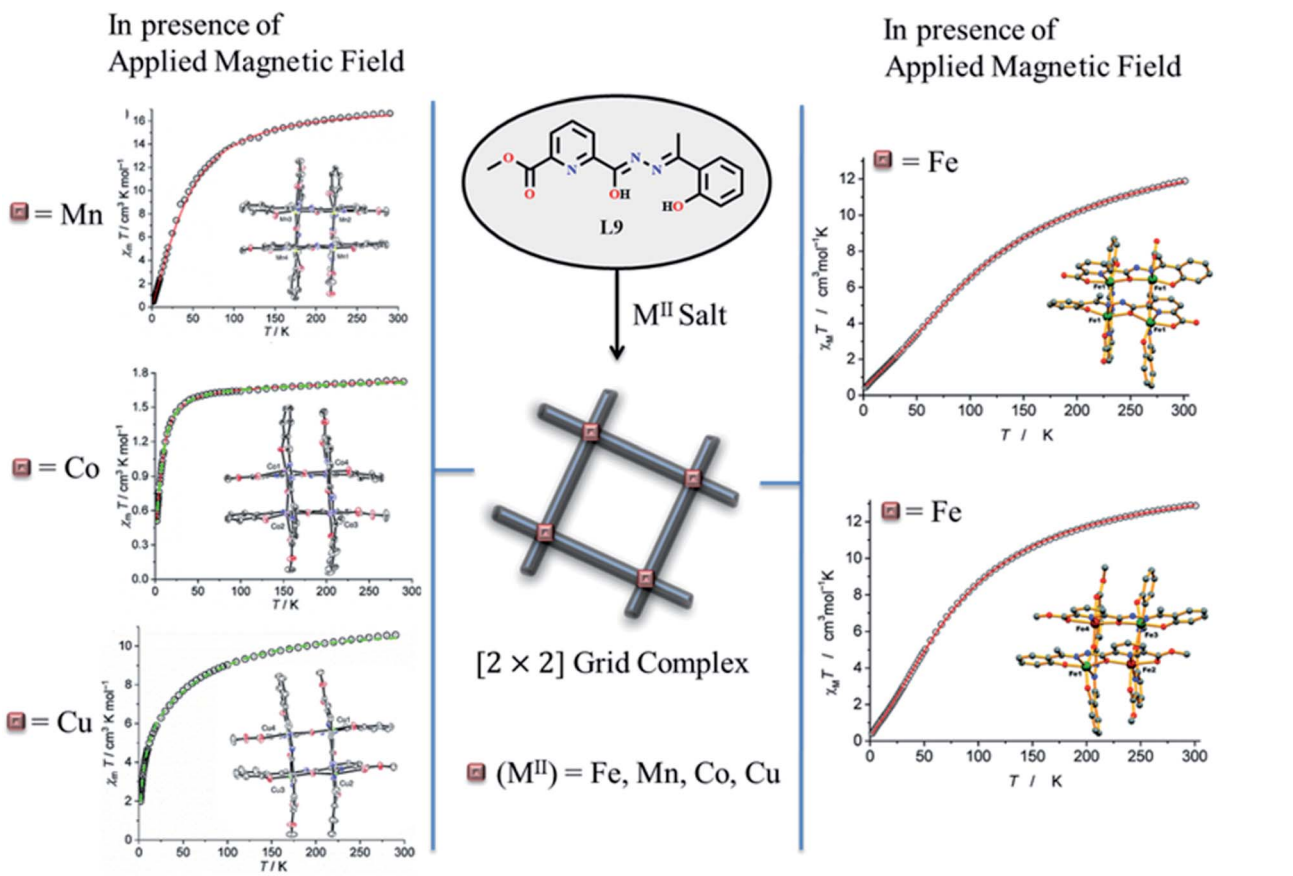

Fig. 9 Magnetic properties and the formation of [2 × 2] $[M_4(\mathbf{L9})_4]$ (M = Fe, Mn, Co, Cu) grid complexes by utilizing the ligand **L9**. Modified and reproduced by permission from ref. 52 and 9, ©2017 and 2019 respectively, The Royal Society of Chemistry.

and **FeL9[a]** were dropped to 0.44 and 0.41 $cm^3\ mol^{-1}$ K. This indicated the presence of antiferromagnetic coupling. In 2019, with the same unsymmetrical ditopic ligand L9, tetranuclear [2 × 2] grid complexes were synthesized with M = Mn^{II}, Co^{II}, Cu^{II} and Zn^{II} by using its two coordination pockets (N_2O_4) and corresponding complexes $[M_4(\mathbf{L9})_4]$ showed antiferromagnetic interactions (Fig. 9).[9]

It is well-known that pyridine-based ligands, due to their easy functionalization, are the most reported ligands for the syntheses of multimetallic complexes. So, contemplating, designing, and working with such ligands will never stop and some more recently reported potential ligands suitable for the current review are highlighted below.

Shao-Min *et al.* in 2021 reported one pyridine-based symmetrical ligand **L10** and its three dysprosium complexes with different salts of Dy^{III} ion.[53] Two of these complexes were mononuclear $[Dy(\mathbf{L10})(H_2O)](ClO_4)\cdot 2CH_3CH_2OH$ (**DyL10[a]**), $[Dy(\mathbf{L10})(NO_3)]$ (**DyL10[b]**) while one of them was dinuclear $[Dy_2(\mathbf{L10})(dbm)_4]$ (**DyL10[c]**, Hdbm = dibenzoylmethane) in nature. Dy(III) centers in **DyL10[a]** and **DyL10[c]** were octa-coordinated in nature with triangular dodecahedron geometry around the metal center, while **DyL10[b]** was nine coordinated in nature and exhibited a spherical capped square antiprism geometry around the metal center. The dimeric form of **DyL10[a]** was attributed to the hydrogen bonding interaction between the inner sphere water molecules, while in **DyL10[c]**, it was due to the phenoxy oxygen atoms, which linked two Dy(III) centers. In **DyL10[a]** and **DyL10[b]** at 300 K, the χ_mT values were found to be 13.24 and 14.17 $cm^3\ mol^{-1}$ K respectively. Further, with decreasing temperature these values smoothly decreased to 12.11 $cm^3\ mol^{-1}$ K for **DyL10[a]** at 22.56 K and to 13.06 $cm^3\ mol^{-1}$ K for **DyL10[b]** at 12.07 K. On further cooling, χ_mT value of **DyL10[a]** promptly increased to 13.43 $cm^3\ mol^{-1}$ K at 2 K suggested the ferromagnetic interaction between two Dy(III) ions. For **DyL10[b]**, on further cooling χ_mT value slowly increased to 13.17 $cm^3\ mol^{-1}$ K at 5.56 K which further rapidly dropped to 10.31 $cm^3\ mol^{-1}$ K at 2 K. This increase in the magnetic susceptibility was attributed to the weak intermolecular ferromagnetic couplings and the rapid decrease was attributed to the presence of magnetic anisotropy. Similarly, for **DyL10[c]** magnetic susceptibility at room temperature was found to be 27.20 $cm^3\ mol^{-1}$ K and on decreasing the temperature χ_mT value decreased slowly to 23.84 $cm^3\ mol^{-1}$ K at 6.35 K and further acquired a value of 24.38 $cm^3\ mol^{-1}$ K at 2 K. This initial increase is attributed due to the weak intracluster antiferromagnetic interaction and the slight increase suggested the presence of weak intracluster ferromagnetic interaction.

Two Dy^{III}-based mononuclear complexes, obtained from the potential ligand **L11**, [Dy(**L11**)X] (X = Cl, **DyL11[a]**; Br, **DyL11[b]**), were reported by Li Zhu *et.al.* in 2021, which were stable in pentagonal bipyramidal geometries and showed SMM behavior.[54] Introduction of both electron withdrawing and donating groups in the ligand backbone was the driving force for the regulation of magnetic anisotropy and SMM behaviour. Magnetic susceptibilities of these compounds were determined at 2–300 K temperature range under 1 kOe applied magnetic field. At room temperature the χ_mT values for **DyL11[a]** and **DyL11[b]** were found to be 14.05 and 13.77 $cm^3\ mol^{-1}$ K respectively. The decrease of temperature resulted a slow decrease of χ_mT values in both the complexes which decreased sharply around 20 K and at 2 K the χ_mT values were decreased to 7.64 and 4.77 $cm^3\ mol^{-1}$ K respectively for **DyL11[a]** and **DyL11[b]**. The decrease in the χ_mT values mainly attributed to the interaction of magnetic anisotropy of the Dy^{III} systems.

Gholamhossein *et.al.* in 2021 reported an easy-to-synthesize small molecule quinoline-based ligand **L12** and its dinuclear Cu^{II} and Ni^{II} complexes $[Cu_2(qpyzc)_2]$ (**CuL12**) and $[Ni_2(qpyzc)_2]$ (**NiL12**) respectively.[55] The ligand contained one coordination NNN pocket in which either of the metal ions could well-fit and the fourth coordination site was satisfied by the other N of pyrazole moiety from another complex. Both the complexes acquired a distorted square planner geometry and the overall charge of the complexes were balanced from the ligand only. It was observed that the behavior of **NiL12** was diamagnetic, as no EPR signal was observed neither at 298 K nor at 110 K, while **CuL12** was successfully showed its paramagnetic behavior. The magnetic properties of the **CuL12** were inspected in the temperature range of 2–300 K. At 300 K, χ_mT value was found at 0.73 $cm^3\ mol^{-1}$ K, whereas decrease the temperature resulted a decrease in the χ_mT value and reached a value of 0.012 $cm^3\ mol^{-1}$ K at 15 K, which was further saturated at low temperature up to 2 K. This decrease in the χ_mT value with temperature well-indicated the anti-ferromagnetic coupling behavior between two Cu^{II} centers.

A multi-functional cyclam-based ligand **L13** and its complexes with Fe^{II} and Co^{II} ions were prepared by Bohuslav *et.al.* in 2021 and their magnetic properties were studied.[56] Three complexes $[M^{II}(\mathbf{L13})](ClO_4)_2\cdot H_2O$ (M^{II} = Fe (**FeL13**), Co (**CoL13**) or $Fe_{0.4}Co_{0.6}$ (**$Fe_{0.4}Co_{0.6}$L13**)) were prepared and crystal structure revealed that all three had octahedral geometry around the metal center. Magnetic studies revealed the presence of SCO behavior in **FeL13**, which was also found in the mixed complex **$Fe_{0.4}Co_{0.6}$L13**. The **CoL13** complex showed a field-induced single-molecule magnet behaviour and surprisingly this SMM behavior was also found in the mixed complex **$Fe_{0.4}Co_{0.6}$L13**. So, this mixed system was claimed to be the first system allowing SCO phenomenon in combination with field-induced SMM properties. At room temperature the χ_mT values of **FeL13**, **CoL13**, and **$Fe_{0.4}Co_{0.6}$L13** were mentioned as 3.77, 2.68, and 3.14 $cm^3\ mol^{-1}$ K respectively. Lowering the temperature resulted in both Fe^{II} contained complexes **FeL13** and **$Fe_{0.4}Co_{0.6}$L13** to remain in their high spin state up to 215 and 200 K respectively. Afterwards, the regular decrease of χ_mT values suggested the presence of SCO behavior in both complexes. $T_{1/2}$ of **FeL13** and **$Fe_{0.4}Co_{0.6}$L13** were found at 141 K and 128 K respectively (Fig. 10). The low spin behavior of the **FeL13** is well confirmed by the graph after 50 K and there, the constant magnetic moment of 0.03 $cm^3\ mol^{-1}$ K up to 2 K confirmed the completion of high spin to low spin conversion. However, in **$Fe_{0.4}Co_{0.6}$L13** the χ_mT values suggested the presence of equal amount of both paramagnetic high spin Co^{II} and diamagnetic low spin Fe^{II} metal centres and the χ_mT value was almost half of the **CoL13**. The magnetic behavior of **CoL13** was different from other complexes, here there was no basic

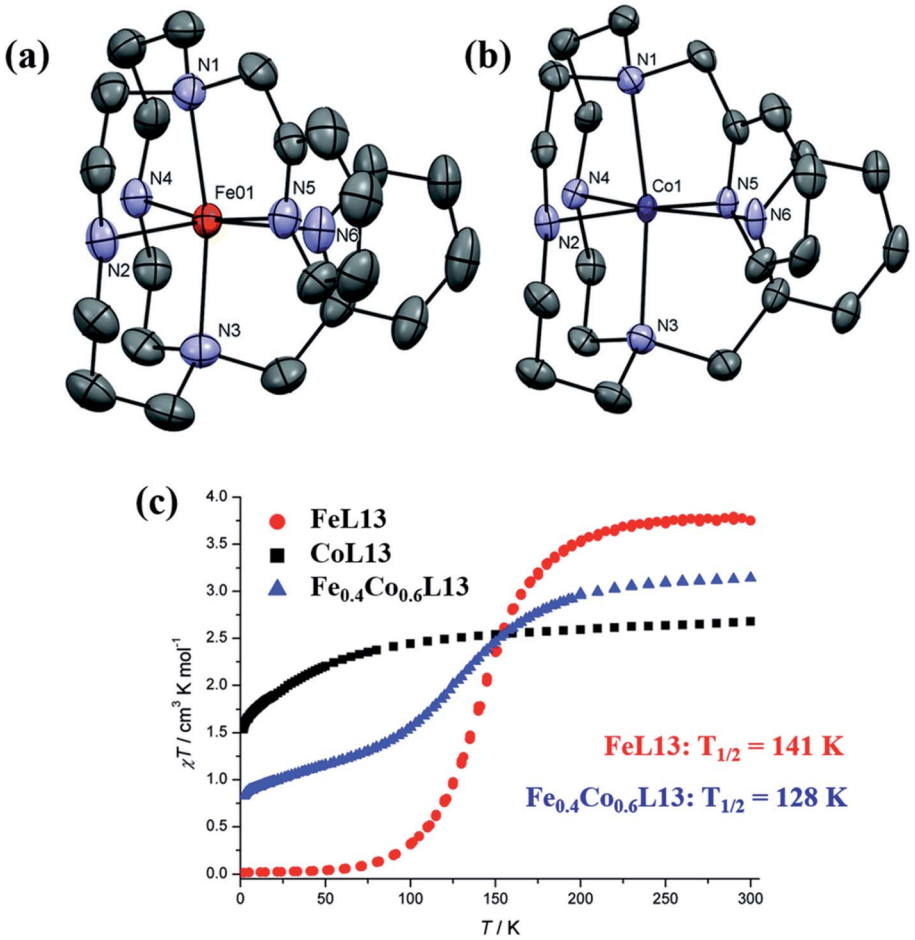

Fig. 10 Single crystal XRD structures of (a) **FeL13** and (b) **CoL13**, showing the binding mode of Fe^{II} and Co^{II} ions by utilizing the ligand **L13** and (c) magnetic properties of **FeL13**, **CoL13**, and $Fe_{0.4}Co_{0.6}$**L13**. Modified and reproduced by permission from ref. 56, ©2021, The Royal Society of Chemistry.

differences in $\chi_m T$ values from 300 K to 100 K and further cooling showed a slow decrease in the $\chi_m T$ values, which was reported to be the fingerprint of zero field splitting (ZFS) effect.

In coordination chemistry six membered heterocyclic diazine-based ligands have a significant class of applications in the area of magnetism.[57–59] Diazine-based ligands can bridge between two metal centres because of their π accepting ability and can withdraw electrons from the metal ion into their aromatic ring to strengthen the metal–ligand interaction by π back bonding. The electrons are withdrawn from the metal ion to an unoccupied π* orbital of the bridging ligand.[60–62] Pyridazine, pyrimidine and pyrazine are also known as 1,2-diazine, 1,3-diazine and 1,4-diazine respectively. Among these three, pyridazine is the strongest and Pyrazine is the weakest base. But these six membered heterocyclic diazines act like weaker bases than pyridine, due to the presence of two nitrogen atom in the ring. So overall basicity order is – pyridine > pyridazine > pyrimidine > pyrazine.[63] These heterocyclic diazines are weak σ donor and good π acceptor. Order of dipole moments of these diazines are – pyridazine > pyrimidine > pyrazine.[64] There are variety of substituted diazine-based ligands present, which act as multidentate and can form binuclear or multinuclear complexes.

3. Pyridazine-based ligands

Pyridazine is a six membered heterocyclic ring, named by scientist Knorr, having direct N–N bond. Broad range of biological and pharmaceutical activities was shown by pyridazine and their derivatives.[65] It shows two Kekule structures and also known as 1,2-diazine or *o*-diaza benzene. It is a colourless liquid at room temperature and has pyridine like odour. It shows a high boiling point (208 °C) and low melting point (−8 °C). Compared to other hydrocarbons these are more easily soluble in water. It shows versatile biological activities for example antiinflammatory,[66,67] analgesic,[68] anticancer,[63] anti-aggregative,[69] antidepressant,[66,67] antihypertensive[70,71] *etc.* 3,6 disubstituted based pyridazine ligands used for the self-assembly grid like metal complex formation,[72] some relevant literature are described below (Scheme 3).

Teresa F. Mastropietro *et al.* in 2012 reported pyridazine based six copper complexes $[Cu(\mathbf{L14})_2(ClO_4)]ClO_4$ (**CuL14**[a]), $[Cu_2(\mathbf{L14})(OH)(ClO_4)_3(H_2O)_3]\cdot H_2O$ (**CuL14**[b]),

$[Cu_2(\mathbf{L14})_2(H_2O)_2](ClO_4)_4$ (**CuL14^c**), $[Cu_2(\mathbf{L14})_2(ClO_4)_4]$ (**CuL14^d**), $([Cu_2(\mathbf{L14})(N_3)_4]\cdot H_2O/[Cu_2(\mathbf{L14})\text{-}(N_3)_4(H_2O)])_n$ (**CuL14^e**) and $([Cu_2(\mathbf{L14})(OH)(dca)_3]\cdot H_2O)_n$ (**CuL14^f**) where **L14** = 3,6-bis(2′-pyridyl)pyridazine and dca = dicyanamide.[73] **L14** when reacts with aqueous solution of copper perchlorate in different ratio 1 : 2, 2 : 1, and 2 : 2 provided different copper based complexes **CuL14^{a-d}** while additional use of azide and dca gave 1D polymers **CuL14^e** and **CuL14^f**. **L14** have two NN coordination pockets, either one or both coordination pockets were used by these complexes and additionally perchlorate, hydroxyl, water, azide and dca groups were used for satisfying the remaining coordination sites of copper. In complex **CuL14^c** and **CuL14^d** both the coordination pockets of **L14** were used and formed binuclear complexes in each case. In which four coordination sites of copper were satisfied by **L14** ligand in 1 : 1 dimeric unit. Variable temperature magnetic measurement explained antiferromagnetic interaction between metal centers in complexes **CuL14^b**, **CuL14^c**, **CuL14^e** and **CuL14^f** (Fig. 11). It is noteworthy to mention that, distance between Cu-N_{pyr} is very less that caused steric hindrance and inhibited the coordination of four copper with four **L14** ligand but when Fe^{II}, Co^{II}, and Ni^{II} were used instead of Cu^{II}, these types of steric hindrances were not observed and lead to form very stable grid complexes, which are explained below.

In 2020, based on 3,6-bis(2′-pyridyl) pyridazine (**L14**) ligand four Ni^{II} complexes (mono-, di-, tri-, and tetranuclear) are reported by Bruno *et al.*[74] Among all four, tetranuclear Ni^{II} complex $[Ni_4(\mu\text{-}\mathbf{L14})_4(\mu\text{-}N_3)_4]Cl_4\cdot 5H_2O$ (**NiL14**) has formed [2 × 2] metallogrid complex and shown a distinct ferromagnetic interaction. **L14** was synthesized by using a published procedure by Butte and Case in 1961.[75] In the structure of tetranuclear **NiL14** complex, hexacoordinated metal centres were presented, in which four coordination sites were satisfied by two **L14** ligands and two coordination sites were occupied by bridging azido groups and formed [2 × 2] metallogrid complex. In the graph χ_mT *vs.* *T*, on cooling, χ_mT value continuously increased and reach to maximum of 10.60 $cm^3\ mol^{-1}$ K at 70 K from 5.0 $cm^3\ mol^{-1}$ K at room temperature and afterwards, it was decreased to 9.40 $cm^3\ mol^{-1}$ K at 1.9 K. Zero field splitting effects or intermolecular antiferromagnetic interaction may be the reason behind the decrease of χ_mT values at 1.9 K.

One more ligand bearing same coordination pockets as **L14** was published by guo *et al.* in 2020 with pyridyl-substituted pyrazine derivative *i.e.*, (**L15**).[76] **L14** and **L15** both formed

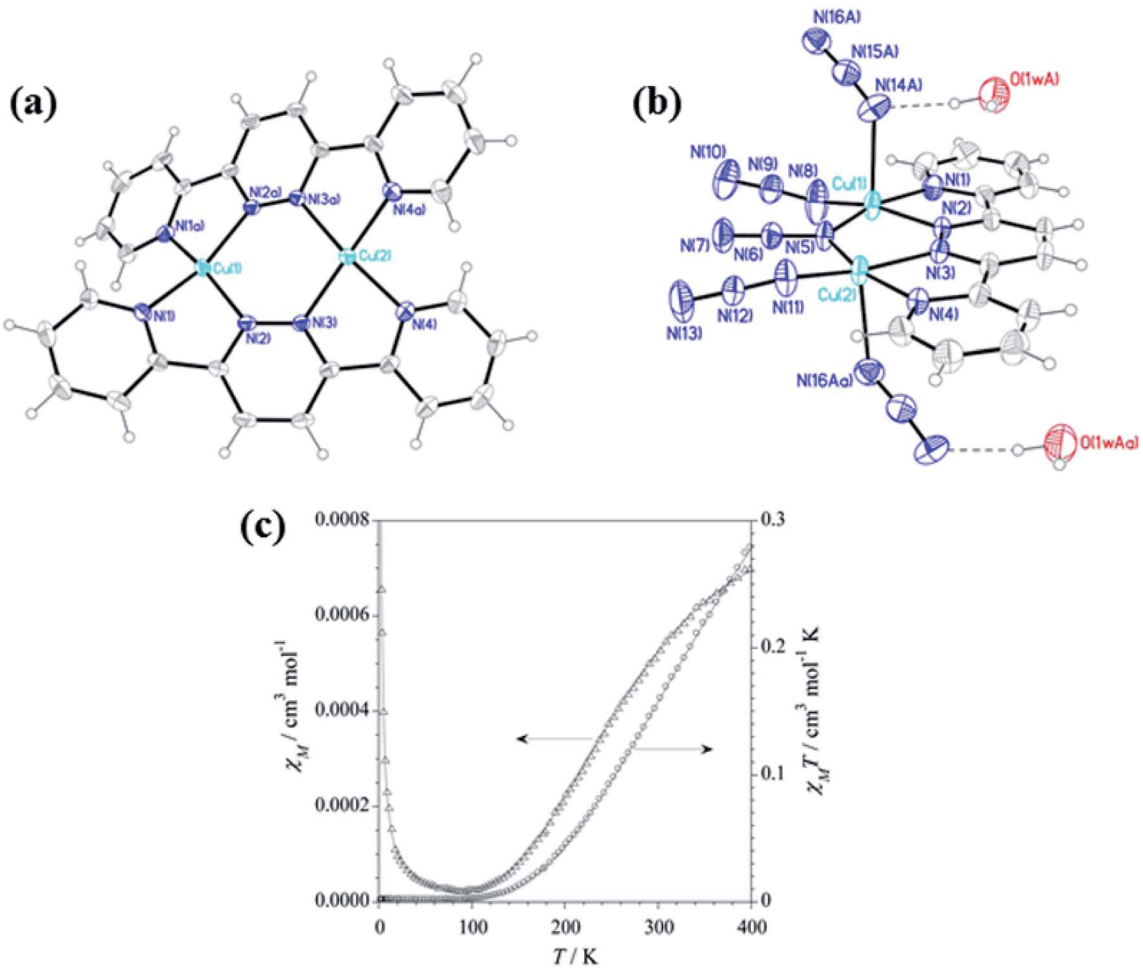

Fig. 11 (a) and (b) represents structure of **CuL14^d** and **CuL14^e**, and (c) represents magnetic behavior of **CuL14^e**. Modified and reproduced with permission from ref. 73 Copyright© 2014, American Chemical Society.

tetranuclear [2 × 2] grid complexes with Co^{II} *i.e.*, ($[Co^{II}_4(\mathbf{L14})_4(N_3)_4]$)·sol (**CoL14**) and $[(\mathbf{L15})_4\ Co^{II}_4(N_3)_4]$)·sol (**CoL15**). Both pyridyl- and pyrazoyl-substituted metallogrid complexes with Co^{II} have shown satisfactory magnetic properties. At 300 K, the χ_mT value for both **CoL14** and **CoL15** are 11.50 and 12.15 $cm^3\ mol^{-1}\ K$ respectively, that sharply increased to 20.26 $cm^3\ mol^{-1}\ K$ (at 12 K) and 25.37 $cm^3\ mol^{-1}\ K$ (at 16 K) respectively, and then dropped to 18.12 and 21.23 $cm^3\ mol^{-1}\ K$ respectively. Such behaviour revealed the presence of ferromagnetic interaction between the metal centers, while the low temperature decrease of χ_mT revealed the presence of intermolecular antiferromagnetic interaction between metal centers (Fig. 12).

Both ligands **L14** and **L15** have huge potentials to show various magnetic behaviors as well as they were structurally suitable for many transition metal complexes to provide grid like structures. Again by using the same ligands **L14** and **L15** and by changing the metal ion to Fe^{II}, same group had published two Fe^{II} grids ($[\mathbf{L14})_4Fe^{II}_4\ (N_3)_4][BPh_4]_4$·sol (**FeL14**)and $[(\mathbf{L15})_4Fe^{II}_4(N_3)_4][BPh_4]_4$·sol (**FeL15**)) in 2021.[77] Among these supramolecular self-assembled complexes, **FeL14** showed spin crossover behavior at 230 K. At 300 K, χ_mT values for both **FeL14** and **FeL15** was found to be 12.34 and 12.77 $cm^3\ mol^{-1}\ K$ respectively. Upon lowering the temperature a gradual decrease in the χ_mT value was identified in **FeL15** until 5 K, which was rapidly decreased to 6.66 $cm^3\ mol^{-1}\ K$ at 2 K. This behavior of **FeL15** was the indication of ZFS or intermolecular antiferromagnetic coupling. In case of **FeL14**, the χ_mT value slowly decreased to 11.5 $cm^3\ mol^{-1}\ K$ upon cooling till 270 K. Then further cooling resulted an abrupt decrease in the χ_mT value to 5.0 $cm^3\ mol^{-1}\ K$ at 200 K. The SCO temperature was estimated to be 230 K. After 200 K, further cooling resulted a gradual decrease in the χ_mT value to 0.59 $cm^3\ mol^{-1}\ K$ at 2 K and this was attributed to the continuous transition to the low spin Fe^{II} state.

Jingjing Lu *et al.* in 2019 reported a pyridazine based Schiff-base ligand which formed three novel dysprosium-based complexes; $[Dy_4(\mathbf{HL16})_2L(DMF)_8]\cdot 2ClO_4CH_2Cl_2\cdot 4DMF(CH_3CH_2)_2O\cdot H_2O$ (**DyL16**[a]), $[Dy_{6\mathbf{L16}3}(PhCOO)_6(CH_3OH)_6]\cdot 11CH_3OH\cdot H_2O$ (**DyL16**[b]) and $[Dy_{10}Na_{2\mathbf{L16}4}(\mu_3\text{-}OH)_4(DMF)_{12}(NO_3)_6]\cdot 6NO_3\cdot 2DMF(CH_3CH_2)_2O\cdot H_2O$ (**DyL16**[c]).[78] Synthesized pyridazine based ligand **L16** reacted with dysprosium salts in different reaction conditions with varying molar ratio provided different dysprosium complexes (Fig. 13). Initially, reaction of dysprosium perchlorate with **L16** gave linear tetranuclear triple-stranded helicate **DyL16**[a], when this perchlorate was replaced by benzoate ion in methanol with molar ratio of 2 : 1 gave a hexanuclear triple-stranded helicate **DyL16**[b]. Again, a dual double-stranded helicate **DyL16**[c] was obtained when $Dy(NO_3)_3\cdot 6H_2O$, **L16**, and $NaHCO_3$ react in 2 : 1 : 4 molar ratio in DMF solvent. These lanthanide complexes showed magnetic response in the range of 2–300 K at 1000 Oe magnetic field. Initially at 300 K, 57.31, 84.77, and 140.54 $cm^3\ mol^{-1}\ K$ of χ_mT values were found for **DyL16**[a], **DyL16**[b], and **DyL16**[c] respectively. After decreasing the temperature, χ_mT value of **DyL16**[a] gradually decreased to 48.37 $cm^3\ mol^{-1}\ K$ at 12 K and then suddenly increased to 63.36 $cm^3\ K\ mol^{-1}$ at 2 K. This scenario indicated the possibility of ferromagnetic coupling between the Dy^{III} centers. Moreover, χ_mT values of **DyL16**[b] and **DyL16**[c] were decreased to 78.44, and 127.82 $cm^3\ K\ mol^{-1}$ at a decreased temperature of 50 K, which further decreased to 68.61 and 103.53 $cm^3\ K\ mol^{-1}$ at 2 K respectively. These behaviours of **DyL16**[b] and **DyL16**[c] suggested the weak antiferromagnetic interaction between Dy^{III} centers.

4. Pyrimidine-based ligands

In natural products, drugs, bioactive molecules, supramolecules, biogenetics, and photophysical materials pyrimidine is used as a fundamental structure.[79–85] 4,6-disubstituted pyrimidine based ligands can form self-assembly metallogrid complexes and able to show magnetic properties[86–90] and some of them are described here based on the recent literature (Scheme 3).

In 2012 Worku A. Gobeze *et al.* reported pyrimidine based bis-tetradentate acyclic amine ligand (**L17**) formed by reaction between 4,6-bis(aminomethyl)-2-phenylpyrimidine and 2-

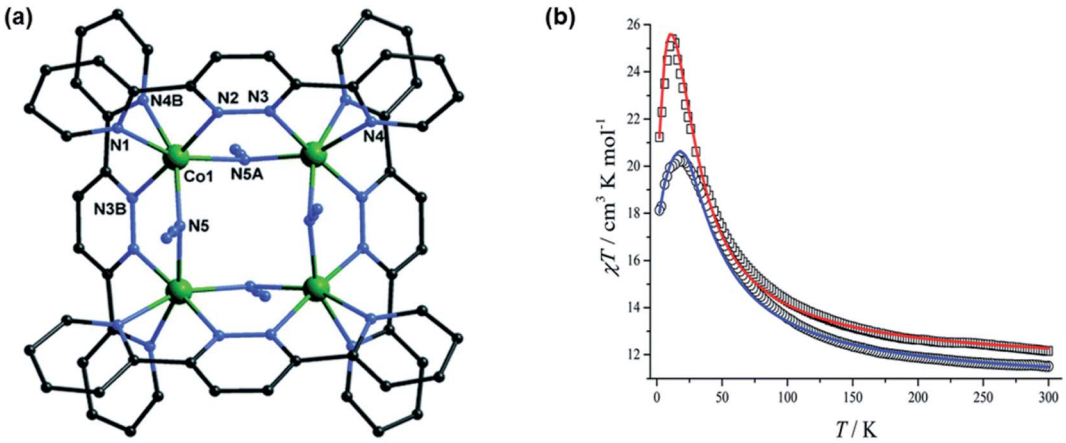

Fig. 12 (a) represents the structure of CoL14 and (b) represents magnetic behaviour of CoL15 (red) and CoL14 (blue). Modified and reproduced with permission from ref. 76, ©2020, the Royal Society of Chemistry.

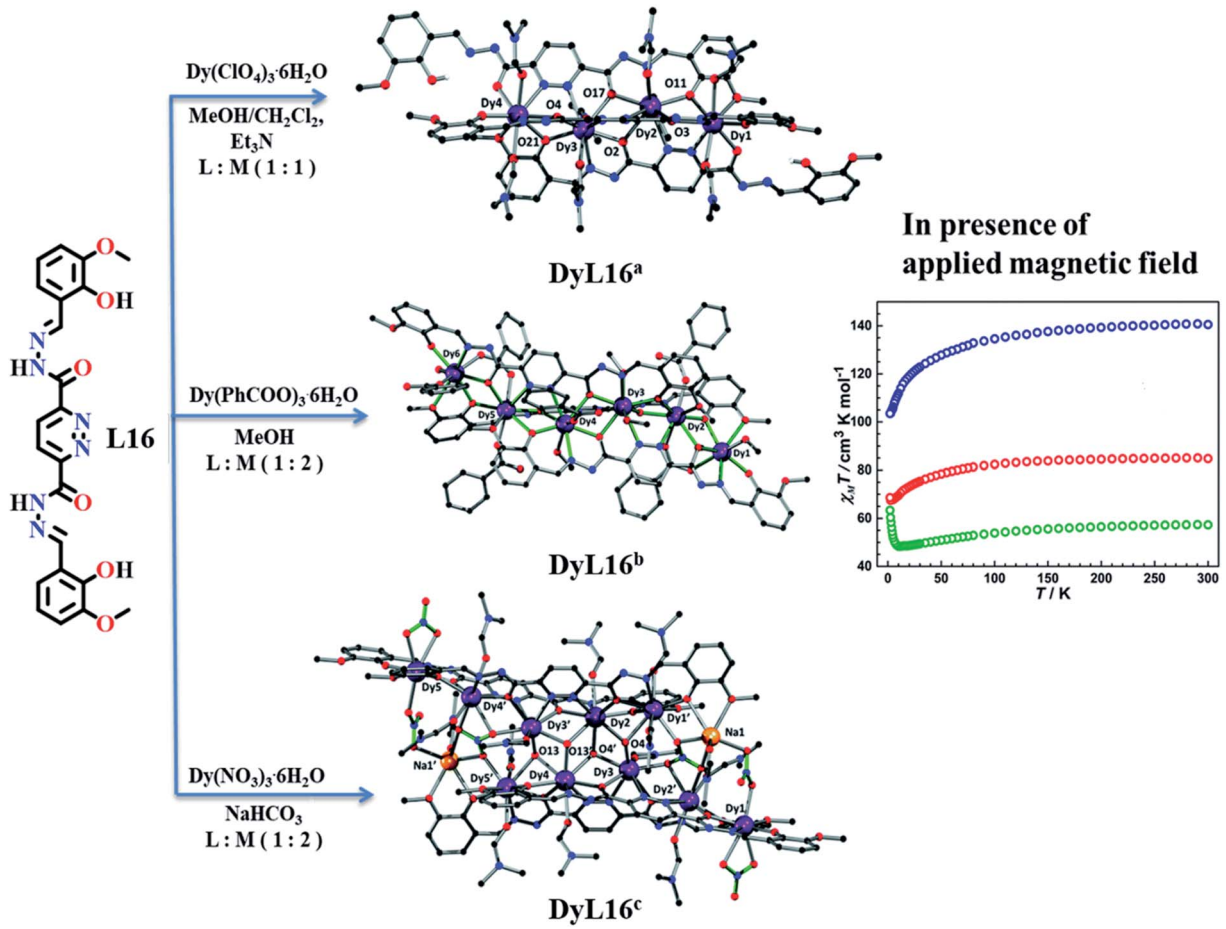

Fig. 13 Formation of different dysprosium complexes from ligand **L16** and their magnetic properties **DyL16**[a] (green), **DyL16**[b] (red), and **DyL16**[c] (blue). Modified and reproduced from ref. 78, © 2019, with permission from the Centre National de la Recherche Scientifique (CNRS) and the Royal Society of Chemistry.

vinylpyridine.[91] On the reaction of **L17** and metal tetrafluoroborate with 1 : 2 molar ratio in MeCN gave dinuclear complexes Fe_2**L17**$(H_2O)_4(BF_4)_4$ (**FeL17**), Co_2**L17**$(H_2O)_3$(MeCN)$_2(BF_4)_4$ (**CoL17**), and Ni_2**L17**$(H_2O)_4(BF_4)_4$ (**NiL17**), while in more protic solvents like MeOH tetranuclear complexes, Fe_4(**L17**)$_2(F)_4(BF_4)_4\cdot 52H_2O$ (**FeL17**[a]), Co_4(**L17**)$_2(F)_4(BF_4)_4\cdot 3H_2O$ (**CoL17**[a]), and Ni_4(**L17**)$_2(F)_4(BF_4)_4\cdot 4H_2O$ (**NiL17**[a]), were formed. In dinuclear and tetranuclear complexes coordination sites of metal centers were satisfied by **L17** in bis-tetradentate fashion (two nitrogen of pyrimidine ring, four nitrogen of pyridine ring and two nitrogen of tertiary amines were coordinated to metal from one ligand). Magnetic susceptibility measurements for all complexes were done in the range of 300 to 2 K. Initially, $\chi_m T$ values of **FeL17**, **CoL17**, **NiL17**, **FeL17**[a], and **NiL17**[a] were 2.3, 2.82, 1.2, 3.6 and 4.47 cm^3 K mol^{-1} respectively, which gradually decreased down as the temperature was lowered. **CoL17**[a] also showed similar type of magnetic behavior in the form of μ_{eff}, which attained a minimum value of 2 μ_B at 2 K. So, plots of $\chi_m T$ *vs.* T and μ_{eff} *vs.* T of these complexes revealed the dominance of antiferromagnetic interaction between metal centers (Fig. 14).

Yi-Tong Wang *et al.* in 2013 reported [2 × 2] metallogrid Fe^{II} complexes with the **L18**.[92] These polynuclear complexes showed spin crossover behaviour. Three [2 × 2] grid-like Fe^{II} complexes $[Fe_4(H$**L18**$^a)_4]Cl_4\cdot 9H_2O$ (**FeL18**[a]), $[Fe_4($**L18**$^a)_2(H_2$**L18**$^a)_2](BF_4)_4\cdot 6H_2O$ (**FeL18**[b]) and $[Fe_4($**L18**$^b)_2(H_2$-**L18**$^b)_2]ClO_4)_4\cdot 4H_2O$ (**FeL18**[c]) were formed by ditopic Schiff base ligands H_2**L18**. All these three complexes were formed by using $FeCl_2\cdot 4H_2O$ metal salt in MeOH solution and for **FeL18**[c] aqueous solution of $NaBF_4/NaClO_4$ was used. All complexes had similar [2 × 2] core grid structure in which all Fe^{II} metal centres were planar except **FeL18**[a] and hexacoordinated with two imine, pyrimidine and pyridine N atoms of the ligand. Magnetic susceptibility experiments confirmed that above 300 K, **FeL18**[a] and **FeL18**[b] showed spin transition from LS to HS state. At 400 K, the observed $\chi_m T$ value was 6.56 emu K mol^{-1} for **FeL18**[a], related to 50% HS Fe^{II} that decreased at 100 K as temperature was decreased. It further decreased at 2 K due to the presence of LS Fe^{II} ions (Fig. 15). Same behaviour was shown by **FeL18**[b] but at 300 K. **FeL18**[c] had shown diamagnetic interactions.

Shu-Qi Wu *et al.* in 2014 reported two tetranuclear Co^{II} metallogrid complexes, and one of them had shown spin crossover behaviour. When the methanolic solution of same ligands (**L18**[a] and **L18**[b]) were reacted with $CoCl_2\cdot 6H_2O$ in aqueous solution of $NaClO_4$, [2 × 2] metallogrid complexes

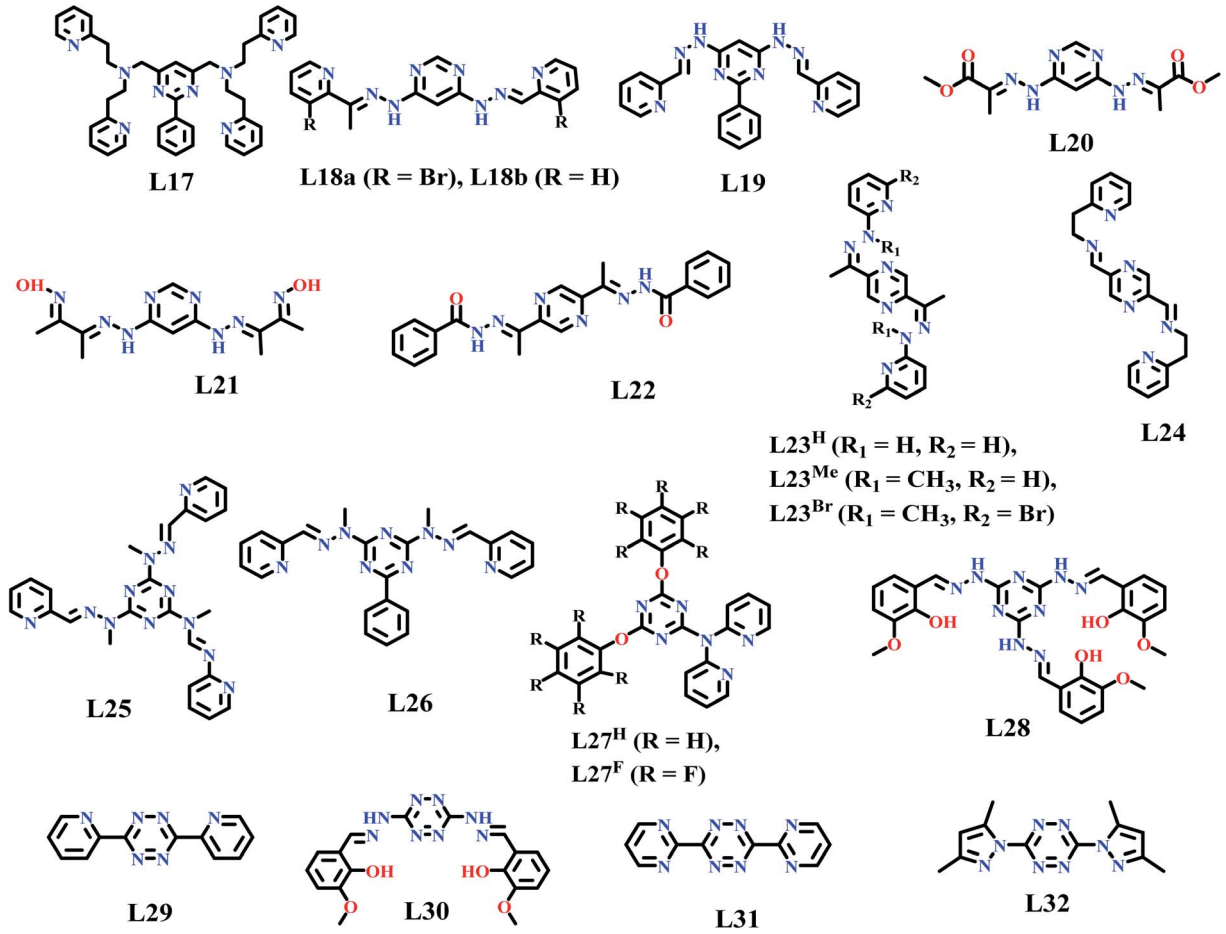

Scheme 3 Pyrimidine, pyrazine, 1,3,5-triazine, and 1,2,4,5-tetrazine based ligands discussed in the present review.

$[Co_4(HL18^a)_4](ClO_4)_4\cdot 8H_2O$ (**CoL18^a**) & $[Co_4(L18^b)_4](ClO_4)_4\cdot 16H_2O$ (**CoL18^b**) respectively were formed.[93] Core structures of both the complexes is very similar, only the deprotonated ligands were different. [2 × 2] grid of **CoL18^a** possessed four octahedral Co^{II} ions and four partially deprotonated ligands $(HL18a)^-$ while **CoL18^b** contained four octahedral Co^{III} ions (t_{2g}^6) and four doubly deprotonated ligands $(L18^b)^{2-}$. Both complexes form a regular 3D packing network that stabilize by H bonds, Br–Br contacts and other intramolecular bonds. The magnetic susceptibility measurements were confirmed that **CoL18^a** had shown the SCO phenomenon in the range of temperature from 2–400 K while **CoL18^b** didn't show such type of phenomenon. At 400 K, χ_mT value of **CoL18^a** was 6.75 emu K mol^{-1} due to presence of 2HS + 2LS Co^{II} ions that gradually decreased on cooling the temperature. At 130 K, decrease in χ_mT value by 2.3 emu was observed due to the presence of 1HS + 3LS Co^{II} ions and further decrease in the χ_mT values attributed to the LS Co^{II} ions. **CoL18^b** complex had shown the temperature independent paramagnetism related to the LS Co^{III} ions (Fig. 16).

L19 was reported in 2018 by Sebastien Dhers *et al.*, which contained two NNN coordination pockets and chelated with two Fe^{II} and Zn^{II} centers.[94] When **L19** was reacted with $Fe(BF_4)_2$ and $Zn(BF_4)_2$ in acetonitrile with required amount of base, [2 × 2] grid complexes were formed, *i.e.*, $[Fe_4(H_2L19)_4](BF_4)_8\cdot x$MeCN (**FeL19^a**), $[Fe_4(H_2L19)_2(HL19)_2](BF_4)_6\cdot 8$MeCN (**FeL19^b**), $[Fe_4(HL19)_4](BF_4)_4\cdot 2$MeCN (**FeL19^c**), $[Zn_4(H_nL19)_4]^{8+}$ (**ZnL19^a**), and $[Zn_4(H_nL19)_4]^{4+}$ (**ZnL19^a**). In these complexes, six coordination sites of each metal center were satisfied by NNN coordination pockets of **L19**, which was arranged around metal centers in perpendicular manner, resulted in the formation of grid complexes. Deprotonated form of ligand **L19** was acted as a strong field ligand and protonated form of **H_2L19** acted as a weak field ligand, that responsible for SCO behavior of these iron complexes. The magnetic properties of these iron complexes were represented in Fig. 17. During magnetic susceptibility measurement it was observed that null magnetic responses were shown by **ZnL19^a** and **ZnL19^a** represented diamagnetic interaction between Zn centers. While iron complexes show magnetic response in magnetic field and their magnetic susceptibility measurements were done in the range of 300–1.85 K. In χ_mT *vs.* T plot, initially at higher temperature χ_mT value of **FeL19^a**, **FeL19^b**, and **FeL19^c** were 6.6, 4.3, and 3.6 cm^3 K mol^{-1} respectively, which were decreased on lowering the temperature and became plateau below 120 K and reached to a minimum value of 2.4, 1.5, and 2.6 cm^3 K mol^{-1} respectively. These types of plot indicated the presence of SCO phenomenon of iron complexes (Fig. 17).

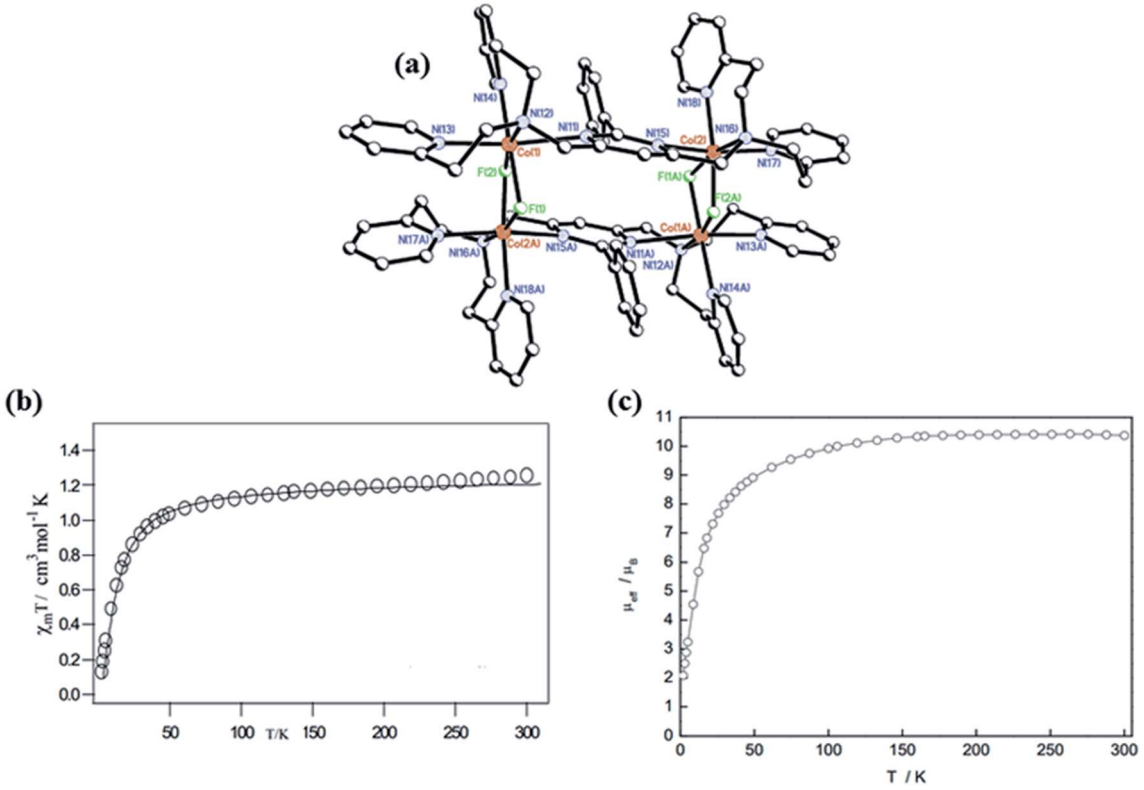

Fig. 14 (a) represents structure of **NiL17**[a], (b) and (c) represents magnetic behavior of **NiL17** and **CoL17**[a]. Reproduced from ref. 91, © 2012, with permission from The Royal Society of Chemistry.

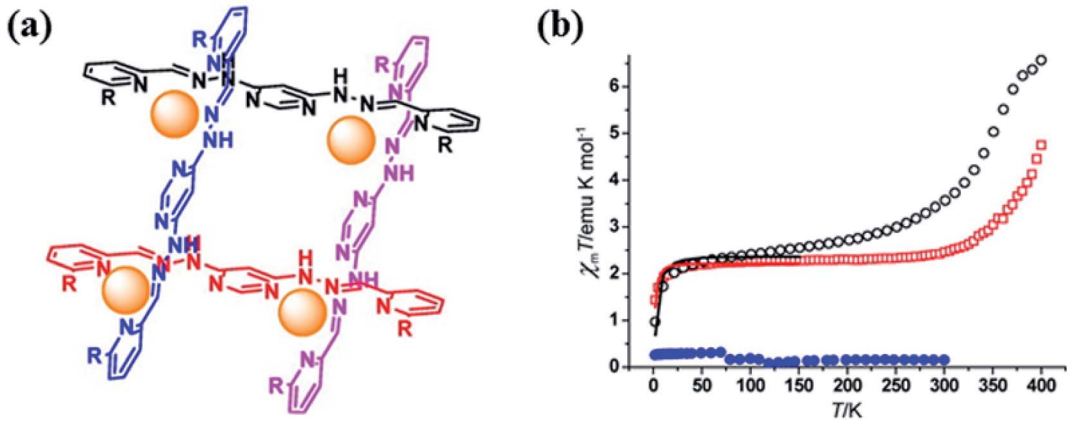

Fig. 15 (a) represents structure of **L18** and (b) represents plot of $\chi_m T$ *vs.* *T* for complex **FeL18**[a] (black), **FeL18**[a] (red) and **FeL18**[a] (blue). Modified and reproduced with permission from ref. 92 Copyright © 2013, American Chemical Society.

Furthermore, to contribute more towards pyrimidine-based metallogrid complexes, Lakma *et al.* in 2018, synthesized ligand **L20** and **L21** by changing the terminal groups of 4,6-dihydrazinylpyrimidine by methyl pyruvate and diacetyl monoxime respectively and both were able to form self-assemble [2 × 2] metallogrid complexes.[95] Two coordination pockets of these ligands were attached with two metal centers and act as hexadentate ligands. These ligands were formed tetranuclear [2 × 2] grid complexes with Ni^{II}, $[Ni_4(\mathbf{L20})_4]\cdot 2CH_3CN\cdot 4CH_3OH\cdot 4H_2O$ (**NiL20**) and $[Ni_4(H_2\mathbf{L21})_4](CF_3SO_3)_8\cdot 4CH_3NO_2\cdot 8H_2O$ (**NiL21**). In the crystal structure of these complexes all six coordination sites of Ni^{II} centres were occupied by two tridentate coordination pockets of two pyrimidine-based ligands [Fig. 18a and 18b]. Magnetic properties of **NiL20** and **NiL21** were shown in Fig. 18c and 18d. Both complexes showed similar type of curve in $\chi_m T$ *vs.* *T* graph. On cooling $\chi_m T$ values of both the complexes were continuously decreased (from 4.80 cm^3 K mol^{-1} for **NiL20** and from 4.43 cm^3 K mol^{-1} for **NiL21**) and below 100 K both the curves were steeply decreased with reaching a value close to 0 cm^3 K mol^{-1} at 2 K, that signified the

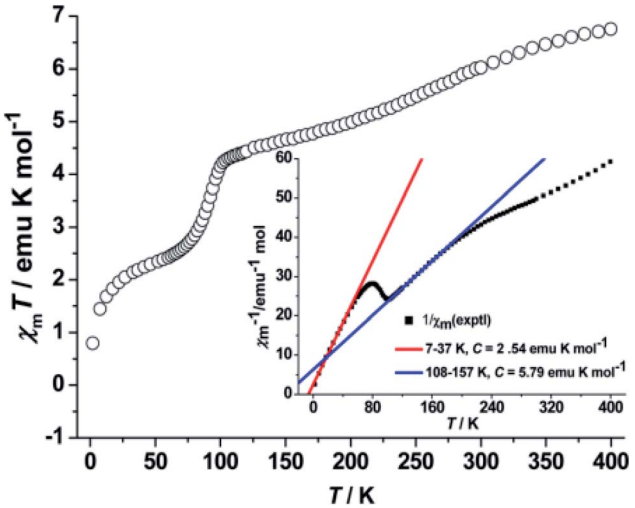

Fig. 16 Plots of $\chi_m T$ *vs.* T and $1/\chi_m$ *vs.* T for **CoL18**[a]. Modified and reproduced with permission from ref. 93 Copyright© 2014, American Chemical Society.

antiferromagnetic exchange interactions between the four centres of a complex.

5. Pyrazine-based ligands

It is an attractive molecule and between two metal centres it can be utilized as a bridging ligand.[96] Functionalization of pyrazine, at 2 and 5 positions, is able to coordinate with 3d octahedral metal ions.[97] 2,5 disubstituted pyrazine based ligands (Scheme 3) could easily be synthesized by Schiff base condensation of pyrazine-2,5-dicarbaldehyde with various primary amines that produced a variety of ligands.[98,99]

Wei Huang *et al.* in 2016 reported two unsymmetrical pyrazine based lanthanide complexes formed *via* self-assembly.[100] Synthesized pyrazine based ligand, pyrazine-2,5-diylbis(ethan1-yl-1-ylidene)di(benzohydrazide)(**L22**), when reacted with $Dy(NO_3)\cdot 6H_2O$ in different solvents different lanthanide complexes were formed. With two equivalents of $Dy(NO_3)\cdot 6H_2O$, binuclear complex $[(Dy_2(\mathbf{L22})(NO_3)_4(DMF)_4]$ (**DyL22**[a]) was formed in presence of NEt_3 and DMF/CH_2Cl_2 and a tetranuclear complex $[Dy_4(\mathbf{L22})_4(H_2O)_4(NO_3)_4]\cdot 6CH_3OH\cdot 6H_2O$ (**DyL22**[b]) was formed when MeOH was used as solvent. By changing the solvent, both dinuclear complexes can be reversibly convertible (Scheme 4). Tetranuclear complex was arranged as [2 × 2] metallogrid structure and this type of example (polynuclear Dy^{III}) is rarely available. In tetranuclear [2 × 2] Dy^{III} metallogrid complex, nine coordination sites of metal centres are satisfied by one water molecule, one chelating nitrate and remaining by two N_2O coordination pockets of the ligand. This tetranuclear grid complex showed magnetic response in 2500 Oe magnetic field in the range of 2–300 K. Initially at 300 K, $\chi_m T$ value was 54.98 $cm^3\ mol^{-1}$ K and after decreasing the temperature, $\chi_m T$ value gradually decreased up to 45.61 $cm^3\ mol^{-1}$ K at 2 K. This type of behaviour revealed the possibility of antiferromagnetic coupling between the Dy^{III} centres which further confirmed by $1/\chi_m$ *versus* T plots that followed Curie–Weiss law with negative value of θ (Fig. 19).

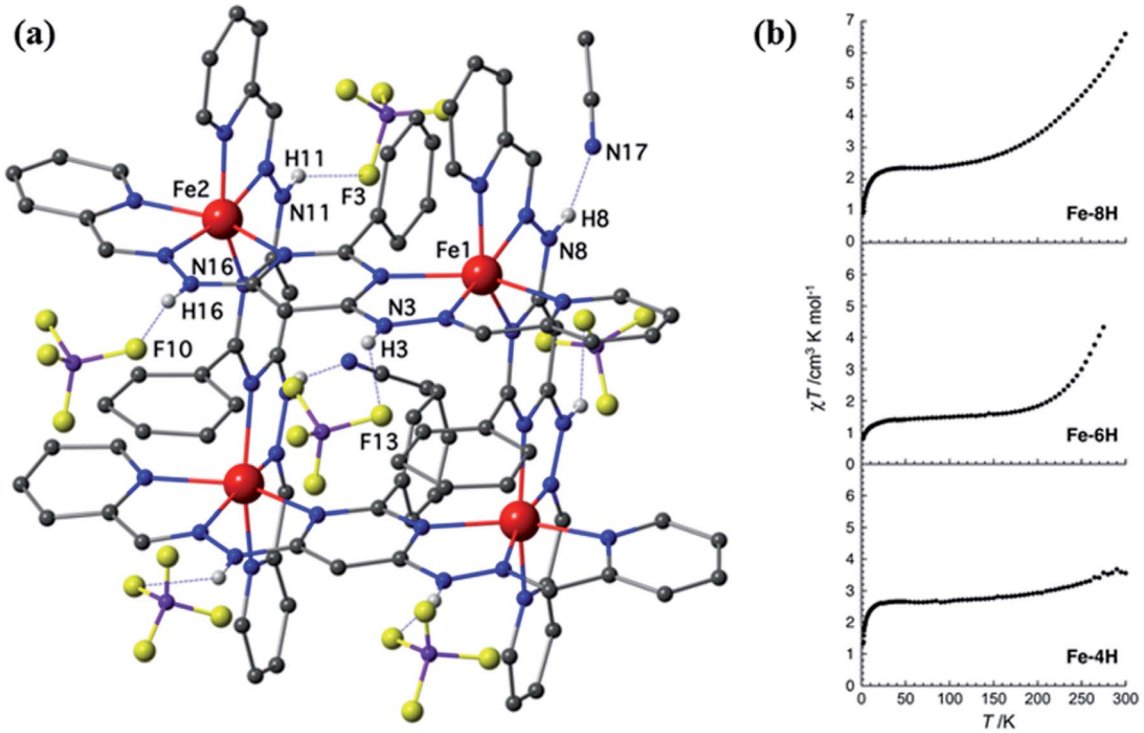

Fig. 17 (a) represents structure of **FeL19**[a] **(Fe–8H)**, and (b) represents magnetic behavior of **FeL19**[a] (Fe–8H), **FeL19**[b] (Fe–6H) and **FeL19**[c] (Fe–4H). Modified and reproduced with permission from ref. 94 Copyright© 2018, American Chemical Society.

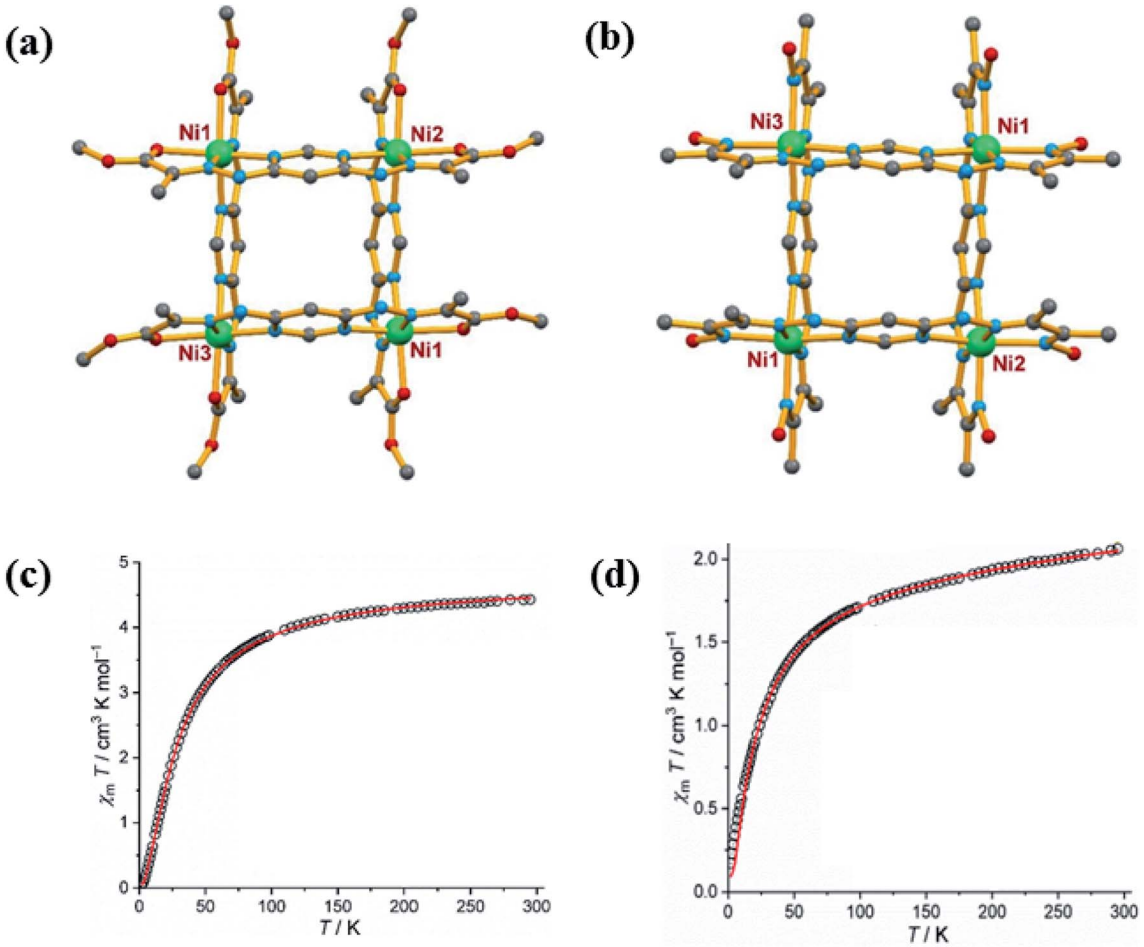

Fig. 18 Structural representation of (a) NiL20 and (b) NiL21, magnetic measurement of (c) NiL20 and (d) NiL21. Modified and reproduced with permission from ref. 95 © 2018 Elsevier B.V. All rights reserved.

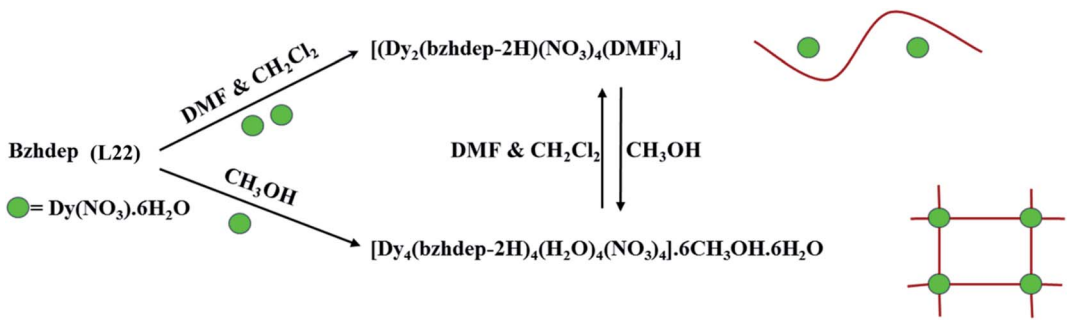

Scheme 4 Represents reversible transformation between a Binuclear Fragment (DyL22[a]) and a tetranuclear metallogrid dysprosium complex (DyL22[b]) in different solvents.

L23 and **L24** have two antiparallel coordination pockets and could able to form [2 × 2] grid complexes with transition metals. **L24** was reported in 2017 by Hogue *et al.* in which it was expected to form a [2 × 2] grid complex, but unexpectedly triangular metal complex was formed with Fe^{II} and Zn^{II}.[101] Conclusion came out from this experiment was that, **L24** type of ligands are flexible in nature like bis-terdentate pyrazine-diamide ligands, and can form [2 × 2] metallogrid complexes. But analogous to this, diamine bis-terdentate pyrazine ligand gives trimetallic triangle architectures.[102–104] **L23** was reported in 2016 by Shen *et al.*, in **L23** (L^H, L^{Me} and L^{Br}) two NNN coordination pockets were present, that chelated with two Co^{II} centres.[105] In complex, each cobalt centre have distorted octahedral environment which formed by using two N atoms of pyrazine, pyridine and hydrazone moiety. So when **L23** (L^H, L^{Me} and L^{Br}) was reacted with $Co(ClO_4)_2{\cdot}6H_2O$, it formed three [2 ×

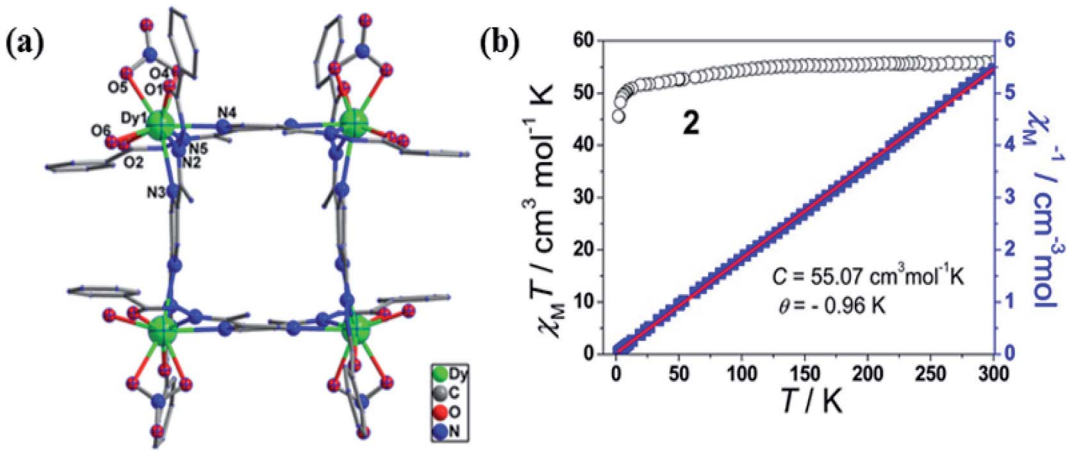

Fig. 19 (a) and (b) represents structure and plot of $\chi_m T$ *vs.* *T* (black) & $1/\chi_m$ *vs.* *T* (blue) for **DyL22**^{b}. Modified and reproduced with permission from ref. 100, Copyright© 2016, American Chemical Society.

2] grid complexes, $[Co_4(\mathbf{L23^H})_4](ClO_4)_4 6DMF\cdot 3H_2O$ (**CoL23^{H}**), $[Co_4(\mathbf{L23^{Me}})_4](ClO_4)_8\cdot 4MeCN\cdot H_2O$ (**CoL23^{Me}**), $[Co_4(\mathbf{L23^{Br}})_4](ClO_4)_8\cdot CH_3OH\cdot 2MeCN\cdot 5H_2O$ (**CoL23^{Br}**). In the applied magnetic field, null magnetic susceptibility was observed for **L23^{H}** complex, that implied low spin Co^{III} grid complex was formed having d^6 configuration. **CoL23^{H}** was found to be diamagnetic however, **CoL23^{Me}** and **CoL23^{Br}** were found to be paramagnetic. In $\chi_m T$ *vs.* *T* plot, on cooling $\chi_m T$ value of both complexes were decreased below 40 K that implied the weak antiferromagnetic interaction between the metal centres. So it is clear that the substituents like R^1, R^2 can affect the magnetic property of a complex (Scheme 5).

6. 1,3,5-Triazine-based ligands

Triazine comes under the class of nitrogen containing heterocycles and among all the well-known triazine is 1,3,5-triazine, also known as s-triazine. Chlorinated derivative of 1,3,5-triazine which is commonly termed as cyanuric chloride ($C_3N_3Cl_3$). The derivatives of cyanuric chlorides are very attracting as they have interesting biological applications in pharmaceutical industry mainly in antimalaric, antibacterial, antifungal, and antineoplastic.[106–108] Various 2,4,6-mono, di and trisubstituted symmetrical and nonsymmetrical derivatives of triazine are formed by swaping of chlorine atoms with different nucleophiles under controlled conditions.[109,110] There are many ligands containing 1,3,5-triazine unit, but only a few 1,3,5-triazine based ligands form grid complexes. In Scheme 3, a variety of 2,4,6-substituted triazine based ligands are shown. All these ligands are synthesized by the same general method that coordinate with metal in different coordination modes showing different properties like spin crossover, water adsorption, and magnetic properties.

L25 was published by Animesh Das *et al.* in 2011.[111] Three tridentate coordination pockets of **L25** were able to coordinate with three metal centres but due to steric interaction of methyl at hydrazone N atom, **L25** only was able to bind with one Mn^{II} centre by using one N atom of triazine and two binding sites of chelating arms. Corresponding complexes of **L25** with Mn^{II} showed antiferromagnetic properties but failed to form a grid complex. **L26** was reported by Nathalie Parizel *et al.* in 2011.[112] When an equivalent amount of Co^{II} salt was reacted with **L26** both, grid and pincer like complexes were produced.[109] But when it was reacted with Cu^{II}, only the grid complex was

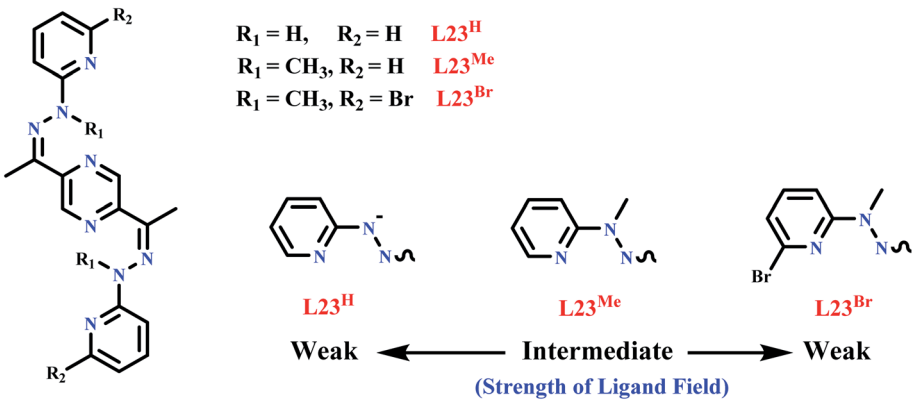

Scheme 5 2,5-disubstituted pyrazine-based ligands used in formation of metallogrid complex.

formed. So, it was concluded that the self-assembly process can be tuned by changing the respective metal ions. Ferromagnetic exchange interaction was displayed by the square [2 × 2] $[Cu_4(\mathbf{L26})_4]^{8+}$ grid complex.

Behaviour of SCO is very interesting in d^6, Fe^{II} ions because high spin states are related with paramagnetic properties while low spin states are related with diamagnetic properties that show applications in optical displays, molecular switches, and data storage devices.[32] Since 2006, for the formation of SCO different types of pyridine based ligands have been designed and synthesized.[113–116] After that s-triazine based SCO compounds were developed.[117] Various dipyridyl amino-substituted-triazine ligands with different nature of transition behaviour were described and developed by Murray and co-workers.[118–121] Again in 2013 Nanthawat Wannarit *et al.* reported the ligand **L27** which was prepared by selective and straightforward substitution of two chlorine atoms of 2,4,6-trichloro-1,3,5-triazine by phenolic compounds and one chlorine atom by 2,2′-dipyridylamine. Surprisingly, its complex with Fe^{II} had shown SCO properties.[33,122] In this ligand, triazine acted as an ancillary ligand and dipyridine group coordinate with the metal centre by its two N atoms. In $[Fe(\mathbf{L27})_2(NCS)_2]\cdot 2CH_2Cl_2$ (**FeL27**), Fe^{II} centre form octahedral geometry in which axial position was occupied by two trans thiocyanate group and equatorial position was occupied by two **L27** ligand shown in Fig. 20. Variable-temperature magnetic susceptibility measurements showed SCO properties of $\mathbf{FeL27^H}$ and $\mathbf{FeL27^F}$ in temperature range 300–5 K shown in Fig. 20(c). At 300 K, $\chi_m T$ value of $\mathbf{FeL27^H}$ was 3.19 $cm^3\ mol^{-1}\ K$ due to the presence of high spin d^6, Fe^{II} complex which decreased upon cooling and at 100 K it reached nearly 0.11–0.07 $cm^3\ mol^{-1}\ K$, that implied the low spin character of d^6, Fe^{II} complex. This SCO behaviour was further supported by its $T_{1/2}$ = 233 K (at 233 K half of the Fe^{II} centres changed their spin state) and ΔT_{80} = 90 K (within 90 K 80% of the transition occurred) value. In case of $\mathbf{FeL27^F}$, initially at 280 K, $\chi_m T$ value was 3.18 $cm^3\ mol^{-1}\ K$, which immediately reduced to 0.1–0.2 $cm^3\ mol^{-1}\ K$ when temperature was reduced to 200 K. Its $T_{1/2}$ and ΔT_{80} value was found to be 238 K and 50 K respectively.

In 2019 Jingjing Lu *et al.* reported triazine based six tetranuclear Dy^{III} complexes $[Dy_4(\mathbf{L28})_2(CH_3OH)_3(NO_3)_3]\cdot 3NO_3\cdot 2H_2O$ ($\mathbf{DyL28^a}$), $[Dy_4(\mathbf{L28})_2(CH_3OH)_2(SCN)_4(OCH_3)_2]\cdot 2CH_3OH\cdot 2H_2O$ ($\mathbf{DyL28^b}$), $([Dy_4(\mathbf{L28})_2(CH_3OH)(SCN)_6(CH_3CN)]\cdot 3CH_3OH\cdot 4CH_3CN)_2$ ($\mathbf{DyL28^c}$), $[Dy_4(\mathbf{L28})_2(CH_3OH)_2(SCN)_6]\cdot 6CH_3OH\cdot 2H_2O$ ($\mathbf{DyL28^d}$), $[Dy_4(\mathbf{L28})_2(CH_3OH)_2(SCN)_4(OCH_3)_2]\cdot 5CH_3OH\cdot 2H_2O$ ($\mathbf{DyL28^e}$), and $[Dy_4(\mathbf{L28})_2(CH_3OH)(SCN)_5(H_2O)_2]\cdot SCN\cdot 4CH_3OH\cdot 2H_2O$ ($\mathbf{DyL28^f}$).[123] All these tetranuclear complexes were obtained by reacting the ligand **L28** with respective salts of dysprosium using different solvents. In $\mathbf{DyL28^{a–c}}$ and $\mathbf{DyL28^{d–f}}$, Dy^{III} centers were octa-coordinated in nature and showed a pseudo-D_{4d} symmetry environment (Scheme 6 and Fig. 21a). For $\mathbf{DyL28^{a–c}}$ magnetic susceptibility measurements are shown in Fig. 21b in which initially, the observed $\chi_m T$ values were 56.82, 56.35, and 58.24 $cm^3\ mol^{-1}\ K$ respectively, and those gradually decreased on lowering the temperature and at 18 K these values reached 51.08, 49.20, and 52.33 $cm^3\ mol^{-1}\ K$ respectively. On further cooling, the $\chi_m T$ values suddenly increased at 2 K and reached to 58.05, 62.66,

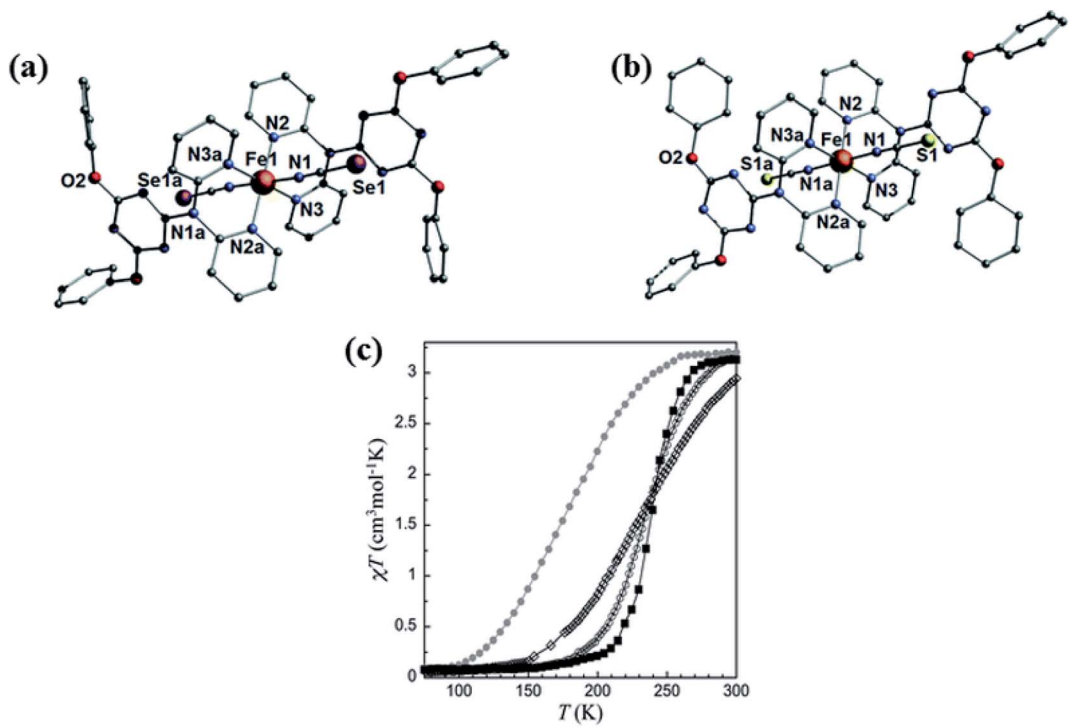

Fig. 20 Structural representation (a) $\mathbf{FeL27^H}$ and (b) $\mathbf{FeL27^F}$ and (c) variable temperature magnetic susceptibility measurement of ($\mathbf{FeL27^H}$ empty circle and $\mathbf{FeL27^F}$ full square). Modified and reproduced with permission from ref. 33, © 2013, The Royal Society of Chemistry.

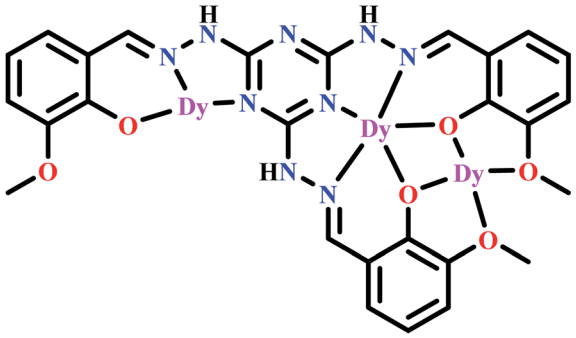

Scheme 6 Coordination mode of L28.

and 61.76 cm^3 mol^{-1} K respectively. These observed values revealed the presence of ferromagnetic interaction and also same type of behaviour was found for the complexes **DyL28**[d–f].

7. 1,2,4,5-Tetrazine-based ligands

1,2,4,5-tetrazine or *s*-tetrazine (TTZ) is one of the most interesting N-heterocyclic ligands. The chemistry of 1,2,4,5-tetrazine (TTZ) heterocyclic is interesting due to four sp^2 nitrogen atoms present in the ring. It has good electron accepting properties which facilitates the formation of its stable radical anions.[124–130] Due to its poor basic property, coordination ability of TTZ is low. It is a weaker base than triazine, and the basicity of tetrazine was never determined but it was estimated that *s*-tetrazine has pK_a value on the order of −6 (for *s*-triazine pK_a = −1.7).[131] Tetrazine can be functionalised at 3,6 position which can develop various types of ligands and can coordinate with same or different type of metal ions. On the basis of substituents on 3 and 6 positions TTZ may be classified in two parts, symmetric TTZ ligands and non-symmetric TTZ ligands. Ditopic dipyridyl and dipyrimidyl tetrazines are mostly used as symmetric ligands. Dipyridyl tetrazine is more developed compared to dipyrimidyl tetrazine in coordination chemistry. Excellent photoluminescence properties may be shown by coordination polymers that are incorporated with bis(pyridyl) tetrazine ligands, because tetrazine acts as a typical organic chromophore.[132] In Scheme 3, a variety of 1,2,4,5-tetrazine based ligands were highlighted. Dimensionality of the resulting coordination compounds can be influenced by the position of nitrogen atom in the pyridyl substituents. 3,6-bis(4-pyridyl)-1,2,45-tetrazine (4,4′-bptz), 3,6-bis(3-pyridyl)-1,2,45-tetrazine (3,3′-bptz), and 3,6-bis(2-pyridyl)-1,2,45-tetrazine (2,2′-bptz) type ligands can enable coordinations in different manner.[133]

In 2017 Brian S. Dolinar *et al.* reported **L29**-based dinuclear lanthanide complexes, $[Dy(tmhd)_3]_2$(**L29**) (**DyL29**[a]) and (Cp_2-Co)($[Dy(tmhd)_3]_2$(**L29**)) (**DyL29**[b]) (tmhd = 2,2,6,6-tetramethyl-3,5- heptane dionate).[134] **DyL29**[a] was formed by the reaction of stoichiometric amount of **L29** and $Dy(tmhd)_3$ in DCM solvent and **DyL29**[b] was synthesized in toluene by the same method with the extra addition of Cp_2Co. Eight coordination sites of Dy^{III} in **DyL29**[a] was satisfied by two NN coordination pockets of **L29** and remaining six sites were occupied by three tmhd ligands. **DyL29**[b] has similar type of coordination environment like the neutral complex **DyL29**[a], except the counter cation part $(Cp_2Co)^+$ and formed [**DyL29**[b]]$^-$ anion. Magnetic susceptibility measurements of both complexes were done in the range of 300–2 K under an applied magnetic field 1000 Oe. Both complexes have similar type of coordination environment but showed different types of magnetic properties. Initially at 300 K, $\chi_m T$ values of **DyL29**[a] and **DyL29**[b] were found to be 27.0 and 33.4 emu K mol^{-1} respectively, which decreased on lowering down the temperature to 10 K and 26 K respectively. After that, $\chi_m T$ value for **DyL29**[a] sharply decreased to 18.7 emu K mol^{-1} at 2 K while for **DyL29**[b] a sudden increase in the $\chi_m T$ value, 42.8 emu K mol^{-1} was observed at 2 K. Finally, plot of $\chi_m T$ *vs.* *T* graph revealed the presence of antiferromagnetic coupling in **DyL29**[a] and ferromagnetic coupling in **DyL29**[b] (Fig. 22).

The first 2,2′-bptz (**L29**) radical bridged Co^{II} square complex was reported by the same group in 2017.[135] In complex $[Co_4$(-**L29**$)_4$(dbm)$_4]\cdot$4MeCN, 1,3-diphenyl-1,3-propanedionate (dbm) was used as auxiliary chelating ligand. 2,2′-bptz formed [2 × 2] grid complex with cobalt in which Co^{II} centres had distorted octahedral environment. Four coordination sites were satisfied by **bptz** ligand and remaining two sites are satisfied by dbm ligand. Magnetic behaviour of the complex showed that χ_mT value gradually increased upon cooling the temperature to 60 K, (Fig. 23b), after that it suddenly decreased to 2.72 cm^3 K mol^{-1}

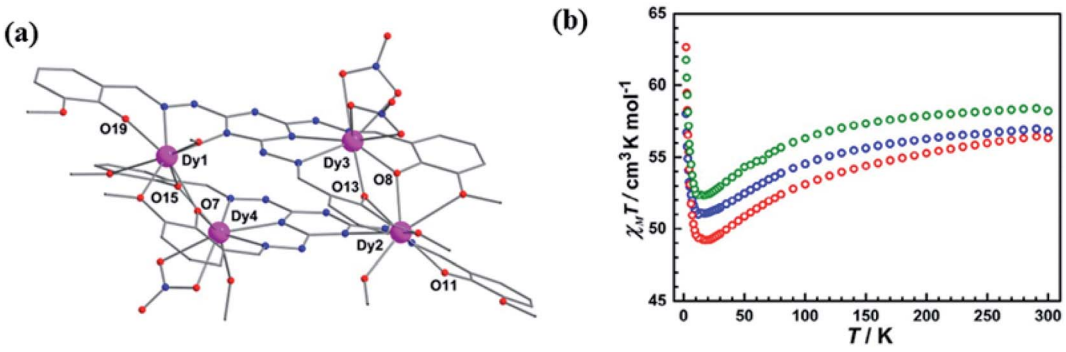

Fig. 21 (a) Structure of **DyL28**[a] and (b) $\chi_m T$ *vs.* T plot for **DyL28**[a] (green), **DyL28**[b] (blue) and **DyL28**[c] (red). Modified and reproduced with permission from ref. 122, Copyright© 2019, American Chemical Society.

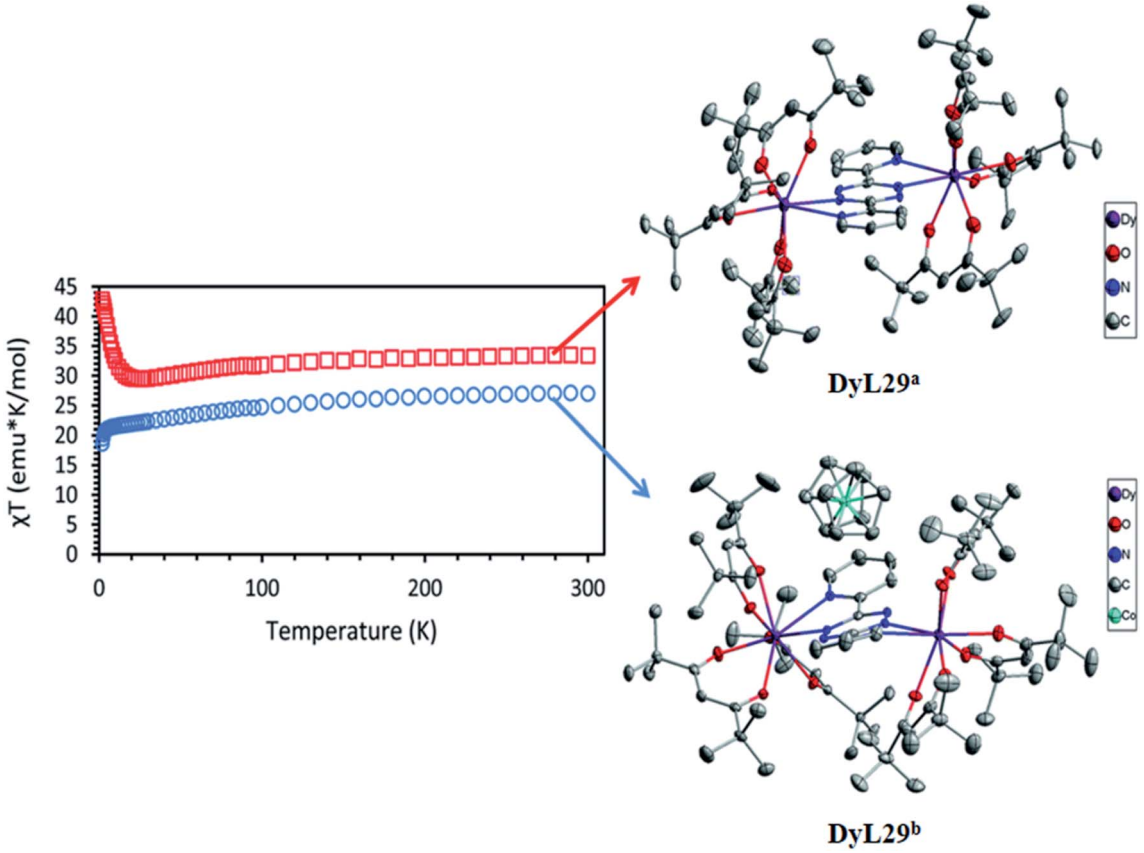

Fig. 22 Structure and magnetic behavior of DyL29[a] (blue circle) and DyL29[b] (red square). Modified and reproduced by permission from ref. 133, © 2017, The Royal Society of Chemistry.

at 2 K, which indicated the existence of antiferromagnetic interaction between the **bptz** radical and Co^{II} ions (Fig. 23).

In 2017 T. Lacelle *et al.* reported two tetranuclear complexes $[Ln_4(\mathbf{L30})_4(MeOH)_8](NO_3)_4 \cdot aMeOH \cdot bH_2O$, where Ln = Dy^{III} (a = 8.07, b = 0.65) (**DyL30[a]**), and Gd^{III} (a = 8.19, b = 0.91) (**DyL30[b]**), based on 3,6-bis(vanillidenehydrazinyl)-1,2,4,5-tetrazine (**L30**), which were formed by the reaction between **L30** and $M(NO_3)_3 \cdot H_2O$ (M = Dy, Gd) in presence of NaN_3 in MeOH solvent.[136] **L30** contained two large NNO coordination pockets with two N of tetrazine, two N of hydrazone moiety and two O from vanilidine moiety suitable for satisfying the coordination sites of lanthanide ions, **L30** also contained two small OO coordination pockets from vanilidine moieties. Tetranuclear complex contained two subunits, in which higher coordination pockets of two ligands were used. These two subunits were linked by using another two ligands with distinct coordination pockets consisting oxygen atom of vanillidine moiety and nitrogen of hydrazone moiety. Both complexes **DyL30[a]** and

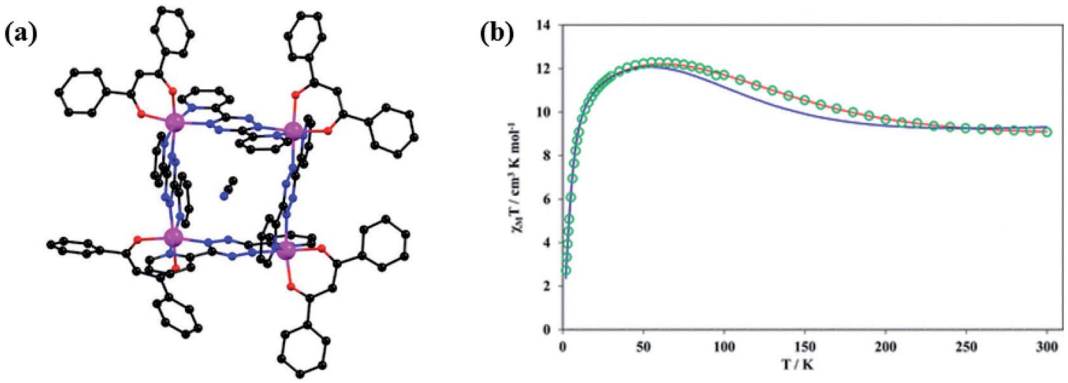

Fig. 23 (a) Structural representation (Co = magenta, O = red, N = blue, C = black) and (b) $\chi_m T$ *vs.* T plot of [2 × 2] grid complex of $[Co_4(\text{-L29})_4(dbm)_4] \cdot 4MeCN$. Modified and reproduced with permission from ref. 134, Copyright© 2017, American Chemical Society.

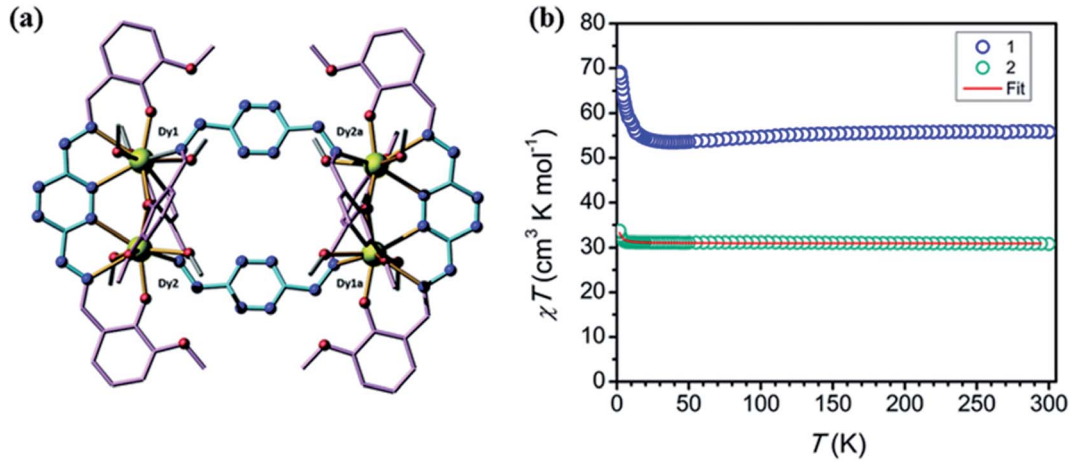

Fig. 24 (a) represents structure of **DyL30**[a] and (b) represents magnetic behavior of **DyL30**[a] and **DyL30**[b]. Modified and reproduced by permission from ref. 135, © 2017, The Royal Society of Chemistry.

DyL30[b] showed magnetic response under 1000 Oe applied field. Initially at 300 K, $\chi_m T$ values of **DyL30**[a] and **DyL30**[b] were observed as 55.81 cm^3 K mol^{-1} and 30.81 cm^3 K mol^{-1} respectively and after decreasing the temperature, $\chi_m T$ values of both complexes remained constant up to 12 K and then suddenly increased at 1.9 K with $\chi_m T$ values, 63.86 cm^3 K mol^{-1} and 33.73 cm^3 K mol^{-1} respectively. This indicated the possibility of ferromagnetic coupling between the metal centers (Fig. 24).

3,6-bis(2-pyrimidyl)-1,2,4,5-tetrazine (**L31**) ligand has four coordination pockets and can coordinate with four metal centres. In 2017 by Lemes *et al.* first example of **L31** radical-based complex $[Ni_4(\mathbf{L31}^{\bullet-})Cl_6(DMF)_8]Cl\cdot 0.5(H_2O)$ (**NiL31**) was published in which all donor atoms of ligand were coordinated with the metal centre.[137] In the complex, each Ni atom had an octahedral environment in which two coordination sites were occupied by two N donor atoms, two axial positions were taken by DMF molecules and remaining sites were occupied by two chlorine atoms. These chlorine atoms acted as bridging ligands between metal centres (Fig. 25a). Magnetic property of **NiL31** was investigated and susceptibility data were obtained in the range of 300–1.8 K at 1000 Oe. It was observed that, up to 9 K, $\chi_m T$ value monotonically increased upon lowering the temperature which revealed the presence of ferromagnetic interaction (Fig. 25b) between Ni^{II} centres and bridging tetrazinyl radical.[138,139]

In 2020 Maykon A. Lemes *et al.* reported the ligand **L32**, 3,6-bis(3,5-dimethyl-pyrazolyl)-1,2,4,5-tetrazine (bpytz), which provided unique type of pancake bonding between metal centers.[140] Dinuclear complexes, $[Dy^{III}_2(\mathbf{L32})(THMD)_6]\cdot 4(C_6H_6)$ (**DyL32*a***), $[Dy^{III}_2(\mathbf{L32})_2(THMD)_4]$ (**DyL32b**), and $[Y^{III}_2(\mathbf{L32})_2(THMD)_4]$ (**YL32**) (TMHD = 2,2,6,6-tetramethyl-3,5-heptanedionate) were obtained by the reaction of equivalent amount of **L32** and $M(TMHD)_3$ (M = Dy^{III} and Y^{III}) in benzene solvent under different condition (aerobic and anaerobic condition respectively). In these three complexes coordination sites of metal centers were completed by two chelating pockets of **L32** and remaining sites were satisfied by TMHD. Complexes

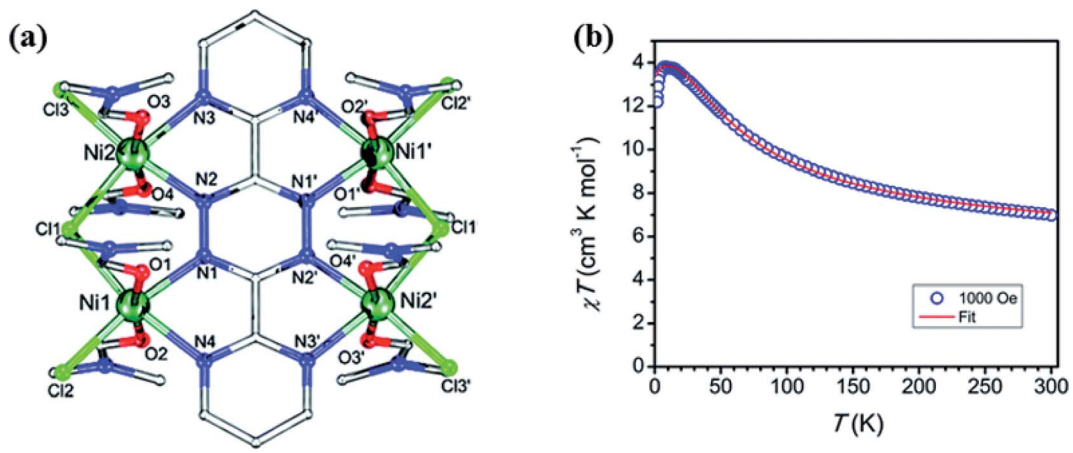

Fig. 25 (a) Structural representation (Ni (green), O (red), N (blue), Cl (light green) and C (grey)) and (b) χ.T *vs.* T plot of **NiL31**. Modified and reproduced by permission from ref. 136, © 2017, The Royal Society of Chemistry.

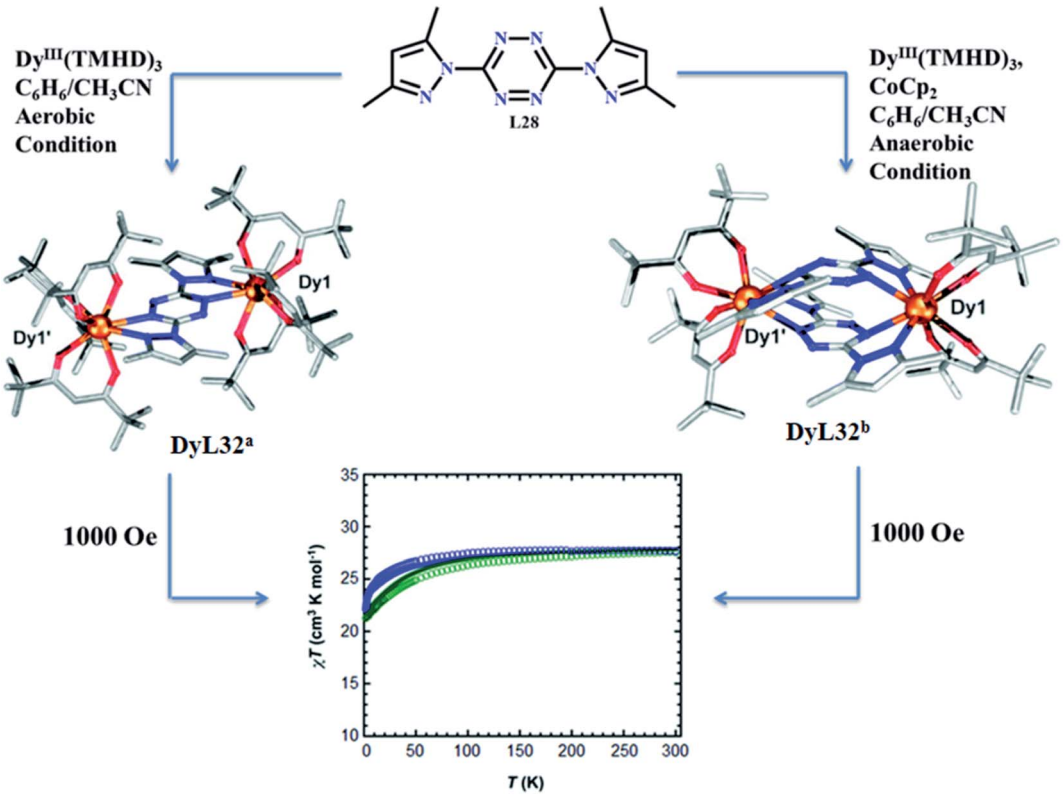

Fig. 26 Structure and magnetic properties of DyL32^a (blue) and DyL32^b (green). Modified and reproduced by permission from ref. 139, © 2020, The Royal Society of Chemistry.

DyL32^b and **YL32** had similar type of structures, in which **L32** was in radical anion form and gave intramolecular pancake type bonding, while in **DyL32*a***, **L32** existed in neutral form. Magnetic studies of **DyL32*a*** and **DyL32*b*** were done under 1000 Oe magnetic field. Initially, at 300 K, χ_mT values of **DyL32^a** and **DyL32^b** were found to be 27.83 and 27.53 cm^3 K mol^{-1} respectively and after lowering down the temperature to 100 K and 50 K, $\chi_m T$ values were not changed and remained constant. This implied the negligible interactions between metal centers. Moreover, further decrease in temperature provided a decrease in $\chi_m T$ values, indicated the weak antiferromagnetic interaction between Dy^{III} centers (Fig. 26).

8. Conclusion and future prospects

This review covers maximum reports on structural and magnetic behaviour of different azabenzene-based ligands published in last 10 years. From the above discussion, it is summarized that N and O atoms containing azabenzene-based aromatic ligands show unique chemistry in coordination complexes. Presence of multiple nitrogen atoms in coordination complexes allows them to interact with suitable substrates that generate supramolecular complexes. This review paper restricts to pyridine, diazine, triazine and tetrazine based ligands. In triazine and tetrazine type, only 1,3,5-triazine and 1,2,4,5-tetrazine are focused due to their strong π acceptor ability as well as symmetrical structures. Magnetic behaviour of the complexes of all the discussed ligands have been highlighted and also their structural representation and coordination pockets to form metallogrid complexes are well explained. Compared to pyridine and diazine based ligands, triazine and tetrazine get little attention as bridging ligand, which is further used for the formation of metallogrid complexes. So, by using different substrates, a variety of azine-based ligands can be made to show different topology and have potential to coordinate with different metal centres to give a homometallic and heterometallic grid complex.

Recently inorganic chemists focus on the synthesis of the ligand systems that give polynuclear clusters and till date very few ligands have been reported on unsymmetrical azine-based ligands. Hydrazone-based ligands were used as powerful precursors for the synthesis of self-assembled polynuclear complexes. Derivatives of azine based ligands form different types of grid complexes and show interesting properties like magnetic, spin crossover phenomena and water absorption *etc.* As most of the reported hydrazone-based ligands show antiferromagnetic interaction with 3d metals, so there is a huge scope for the development of ligands which can show ferromagnetic coupling with 3d metals, or with 3d-4f metals, and can show hysteresis loop because it is advantageous for the development of soft or hard magnets and also can be used in data storage devices. We have tried to cover most of the works related to this field. We extend our regrets to the authors whose work we might have missed in the present review. We sincerely hope

that this article will make an interesting read, provide insights to future researches and studies.

Conflicts of interest

There are no conflicts to declare.

Acknowledgements

AKS acknowledges SERB, India (Grant No. CRG/2020/004334) for funding. JS and SKP acknowledge IIT Bhubaneswar for the fellowship.

References

1 A. Katoh and R. Saito, *J. Synth. Org. Chem., Jpn.*, 2004, **62**, 335–346.
2 E. Fischer, *Ber. Dtsch. Chem. Ges.*, 1894, **27**, 2985–2993.
3 J. M. Lehn, *Angew. Chem., Int. Ed. Engl.*, 1988, **27**, 89–112.
4 J.-M. Lehn, *Angew. Chem., Int. Ed. Engl.*, 1990, **29**, 1304–1319.
5 I. P. Parkin, *Appl. Organomet. Chem.*, 2001, **15**, 236.
6 J. G. Hardy, *Chem. Soc. Rev.*, 2013, **42**, 7881–7899.
7 M. Ruben, J. Rojo, F. J. Romero-Salguero, L. H. Uppadine and J. M. Lehn, *Angew. Chem., Int. Ed.*, 2004, **43**, 3644–3662.
8 L. N. Dawe, K. V. Shuvaev and L. K. Thompson, *Chem. Soc. Rev.*, 2009, **38**, 2334–2359.
9 A. Lakma, S. M. Hossain, J. van Leusen, P. Kögerler and A. K. Singh, *Dalton Trans.*, 2019, **48**, 7766–7777.
10 A. Lakma, S. M. Hossain, R. N. Pradhan, D. Topwal, A. Cornia and A. K. Singh, *Eur. J. Inorg. Chem.*, 2016, **2016**, 2993–2999.
11 J. S. Miller, *Chem. Soc. Rev.*, 2011, **40**, 3266–3296.
12 S. Roy, T. N. Mandal, A. K. Barik, S. Gupta, M. S. E. Fallah, J. Tercero, R. J. Butcher and S. K. Kar, *Dalton Trans.*, 2009, 8215–8226.
13 R. L. Carlin, *Magnetochemistry*, Springer Science & Business Media, 2012.
14 P. W. Selwood, *Magnetochemistry*, Read Books Ltd, 2013.
15 R. Fagaly, *Rev. Sci. Instrum.*, 2006, **77**, 101101.
16 C. Granata and A. Vettoliere, *Phys. Rep.*, 2016, **614**, 1–69.
17 R. Kleiner, D. Koelle, F. Ludwig and J. Clarke, *Proc. IEEE*, 2004, **92**, 1534–1548.
18 K. Enpuku, T. Minotani, M. Hotta and A. Nakahodo, *IEEE Trans. Appl. Supercond.*, 2001, **11**, 661–664.
19 T. Ryhänen, H. Seppä, R. Ilmoniemi and J. Knuutila, *J. Low Temp. Phys.*, 1989, **76**, 287–386.
20 H. Weinstock, *SQUID Sensors: Fundamentals, Fabrication and Applications*, Springer Netherlands, 2012.
21 K. Gramm, L. Lundgren and O. Beckman, *Phys. Scr.*, 1976, **13**, 93.
22 K. R. Meihaus, J. D. Rinehart and J. R. Long, *Inorg. Chem.*, 2011, **50**, 8484–8489.
23 S. Kobayashi, H. Ueda, C. Michioka and K. Yoshimura, *Inorg. Chem.*, 2016, **55**, 7407–7413.
24 P. W. Anderson, *Phys. Rev.*, 1950, **79**, 350–356.
25 P. W. Anderson, *Phys. Rev.*, 1959, **115**, 2–13.
26 M. Speldrich, J. van Leusen and P. Kögerler, *J. Comput. Chem.*, 2018, **39**, 2133–2145.
27 I. de PR Moreira, N. Suaud, N. Guihéry, J.-P. Malrieu, R. Caballol, J. Bofill and F. Illas, *Phys. Rev. B*, 2002, **66**, 134430.
28 W. H. Harman, T. D. Harris, D. E. Freedman, H. Fong, A. Chang, J. D. Rinehart, A. Ozarowski, M. T. Sougrati, F. Grandjean and G. J. Long, *J. Am. Chem. Soc.*, 2010, **132**, 18115–18126.
29 M. Ruben, E. Breuning, J.-M. Lehn, V. Ksenofontov, F. Renz, P. Gütlich and G. B. M. Vaughan, *Chem.–Eur. J.*, 2003, **9**, 4422–4429.
30 A. Bousseksou, G. Molnár, L. Salmon and W. Nicolazzi, *Chem. Soc. Rev.*, 2011, **40**, 3313–3335.
31 O. Sato, *Proc. Jpn. Acad., Ser. B*, 2012, **88**, 213–225.
32 P. Gütlich, Y. Garcia and H. A. Goodwin, *Chem. Soc. Rev.*, 2000, **29**, 419–427.
33 N. Wannarit, O. Roubeau, S. Youngme, S. J. Teat and P. Gamez, *Dalton Trans.*, 2013, **42**, 7120–7130.
34 P. P. Pandey, *Pyridine*, IntechOpen, 2018.
35 T. L. S. Kishbaugh, *Progress in Heterocyclic Chemistry*, ed. G. W. Gribble and J. A. Joule, Elsevier, 2012, vol. 24, pp. 343–391.
36 L. N. Dawe, T. S. M. Abedin and L. K. Thompson, *Dalton Trans.*, 2008, 1661–1675, DOI: **10.1039/B716114J**.
37 L. N. Dawe, T. S. M. Abedin, T. L. Kelly, L. K. Thompson, D. O. Miller, L. Zhao, C. Wilson, M. A. Leech and J. A. K. Howard, *J. Mater. Chem.*, 2006, **16**, 2645–2659.
38 M. U. Anwar, L. N. Dawe, S. R. Parsons, S. S. Tandon, L. K. Thompson, S. K. Dey, V. Mereacre, W. M. Reiff and S. D. Bunge, *Inorg. Chem.*, 2014, **53**, 4655–4668.
39 C. J. Matthews, L. K. Thompson, S. R. Parsons, Z. Xu, D. O. Miller and S. L. Heath, *Inorg. Chem.*, 2001, **40**, 4448–4454.
40 L. Zhao, C. J. Matthews, L. K. Thompson and S. L. Heath, *Chem. Commun.*, 2000, 265–266, DOI: **10.1039/A909180G**.
41 O. Waldmann, H. U. Güdel, T. L. Kelly and L. K. Thompson, *Inorg. Chem.*, 2006, **45**, 3295–3300.
42 J. Hou, *Acta Crystallogr., Sect. E: Struct. Rep. Online*, 2008, **64**, m1571.
43 V. Chandrasekhar, S. Hossain, S. Das, S. Biswas and J.-P. Sutter, *Inorg. Chem.*, 2013, **52**, 6346–6353.
44 S. Biswas, S. Das, J. van Leusen, P. Kögerler and V. Chandrasekhar, *Eur. J. Inorg. Chem.*, 2014, **2014**, 4159–4167.
45 A. Adhikary, S. Goswami, J. A. Sheikh and S. Konar, *Eur. J. Inorg. Chem.*, 2014, **2014**, 963–967.
46 J. Wu, L. Zhao, M. Guo and J. Tang, *Chem. Commun.*, 2015, **51**, 17317–17320.
47 P. Zhang, L. Zhang, S.-Y. Lin, S. Xue and J. Tang, *Inorg. Chem.*, 2013, **52**, 4587–4592.
48 X.-L. Li, H. Li, D.-M. Chen, C. Wang, J. Wu, J. Tang, W. Shi and P. Cheng, *Dalton Trans.*, 2015, **44**, 20316–20320.
49 S. Xue, Y.-N. Guo, L. Ungur, J. Tang and L. F. Chibotaru, *Chem.–Eur. J.*, 2015, **21**, 14099–14106.
50 J. Wu, X.-L. Li, M. Guo, L. Zhao, Y.-Q. Zhang and J. Tang, *Chem. Commun.*, 2018, **54**, 1065–1068.

51 S. Biswas, S. Das, S. Hossain, A. K. Bar, J.-P. Sutter and V. Chandrasekhar, *Eur. J. Inorg. Chem.*, 2016, **2016**, 4683–4692.
52 S. M. Hossain, A. Lakma, R. N. Pradhan, S. Demeshko and A. K. Singh, *Dalton Trans.*, 2017, **46**, 12612–12618.
53 S.-M. Xu, Z.-W. An, W. Zhang, Y.-Q. Zhang and M.-X. Yao, *CrystEngComm*, 2021, **23**, 2825–2834.
54 L. Zhu, Y. Dong, B. Yin, P. Ma and D. Li, *Dalton Trans.*, 2021, **50**, 12607–12618.
55 G. Mohammadnezhad, N. Ahfad, S. Meghdadi, H. Farrokhpour, S. Schmitz, A. Haseloer, A. Buchholz, W. Plass and A. Klein, *Eur. J. Inorg. Chem.*, 2021, **2021**, 1786–1795.
56 B. Drahoš, I. Šalitroš, I. Císařová and R. Herchel, *Dalton Trans.*, 2021, **50**, 11147–11157.
57 S. Derossi, M. Casanova, E. Iengo, E. Zangrando, M. Stener and E. Alessio, *Inorg. Chem.*, 2007, **46**, 11243–11253.
58 M. Schweiger, S. R. Seidel, A. M. Arif and P. J. Stang, *Angew. Chem.*, 2001, **113**, 3575–3577.
59 R. P. John, J. Park, D. Moon, K. Lee and M. S. Lah, *Chem. Commun.*, 2006, 3699–3701, DOI: **10.1039/B607675K**.
60 J. S. Gardner, D. P. Strommen, W. S. Szulbinski, H. Su and J. R. Kincaid, *J. Phys. Chem. A*, 2003, **107**, 351–357.
61 F. D. Rochon and M. Fakhfakh, *Inorg. Chim. Acta*, 2009, **362**, 1455–1466.
62 D. P. Ašanin, M. D. Živković, S. Rajković, B. Warżajtis, U. Rychlewska and M. I. Djuran, *Polyhedron*, 2013, **51**, 255–262.
63 R. K. Bansal, *Heterocyclic chemistry*, New Age International, 2008.
64 W. C. Schneider, *J. Am. Chem. Soc.*, 1948, **70**, 627–630.
65 S. Lin, Z. Liu and Y. Hu, *J. Comb. Chem.*, 2007, **9**, 742–744.
66 L. Pitarch, R. Coronas and J. Mallol, *Eur. J. Pharmacol.*, 1974, **9**, 644–650.
67 S. Mirzoeva, A. Sawkar, M. Zasadzki, L. Guo, A. V. Velentza, V. Dunlap, J.-J. Bourguignon, H. Ramstrom, J. Haiech and L. J. Van Eldik, *J. Med. Chem.*, 2002, **45**, 563–566.
68 F. ROHET, C. RUBAT, P. COUDERT, E. ALBUISSON and J. COUQUELET, *Chem. Pharm. Bull.*, 1996, **44**, 980–986.
69 A. Montero-Lastres, N. Fraiz, R. Laguna, E. CANO, I. ESTEVEZ and E. RAVINA, *Biol. Pharm. Bull.*, 1999, **22**, 1376–1379.
70 R. Slater, W. Howson, G. Swayne, E. Taylor and D. Reavill, *J. Med. Chem.*, 1988, **31**, 345–351.
71 R. Buchman, J. A. Scozzie, Z. S. Ariyan, R. D. Heilman, D. J. Rippin, W. J. Pyne, L. J. Powers and R. J. Matthews, *J. Med. Chem.*, 1980, **23**, 1398–1405.
72 S. K. Dey, L. K. Thompson and L. N. Dawe, *Chem. Commun.*, 2006, 4967–4969.
73 T. F. Mastropietro, N. Marino, D. Armentano, G. De Munno, C. Yuste, F. Lloret and M. Julve, *Cryst. Growth Des.*, 2013, **13**, 270–281.
74 R. Bruno, N. Marino, J. Cano, A. P. Alvarez, A. Ben Tama, F. Lloret, M. Julve and G. De Munno, *Cryst. Growth Des.*, 2020, **20**, 6478–6492.
75 W. A. Butte and F. H. Case, *J. Org. Chem.*, 1961, **26**, 4690–4692.
76 Z. Guo, Y.-F. Deng, Y. Zhang, Z. Pikramenou and Y.-Z. Zhang, *Dalton Trans.*, 2020, **49**, 9218–9222.
77 Z. Guo, M. You, Y.-F. Deng, Q. Liu, Y.-S. Meng, Z. Pikramenou and Y.-Z. Zhang, *Dalton Trans.*, 2021, **50**, 14303–14308.
78 J. Lu, X.-L. Li, C. Jin, Y. Yu and J. Tang, *New J. Chem.*, 2020, **44**, 994–1000.
79 L. M. De Coen, T. S. Heugebaert, D. Garcia and C. V. Stevens, *Chemical Reviews*, 2016, **116**, 80–139.
80 W. B. Parker, *Chemical Reviews*, 2009, **109**, 2880–2893.
81 S. R. Walker, E. J. Carter, B. C. Huff and J. C. Morris, *Chemical Reviews*, 2009, **109**, 3080–3098.
82 G. S. Feng, M. W. Chen, L. Shi and Y. G. Zhou, *Angew. Chem.*, 2018, **130**, 5955–5959.
83 N. Aizawa, Y.-J. Pu, H. Sasabe and J. Kido, *Org. Electron.*, 2012, **13**, 2235–2242.
84 A. S. Duerfeldt and D. L. Boger, *J. Am. Chem. Soc.*, 2014, **136**, 2119–2125.
85 J.-Q. Zhang, Y.-J. Luo, Y.-S. Xiong, Y. Yu, Z.-C. Tu, Z.-J. Long, X.-J. Lai, H.-X. Chen, Y. Luo and J. J. Weng, *J. Med. Chem.*, 2016, **59**, 7268–7274.
86 A. R. Stefankiewicz, G. Rogez, J. Harrowfield, A. N. Sobolev, A. Madalan, J. Huuskonen, K. Rissanen and J.-M. Lehn, *Dalton Trans.*, 2012, **41**, 13848–13855.
87 K. V. Shuvaev, L. N. Dawe and L. K. Thompson, *Dalton Trans.*, 2010, **39**, 4768–4776.
88 O. Waldmann, M. Ruben, U. Ziener, P. Müller and J. M. Lehn, *Inorg. Chem.*, 2006, **45**, 6535–6540.
89 X.-Y. Cao, J. Harrowfield, J. Nitschke, J. Ramírez, A.-M. Stadler, N. Kyritsakas-Gruber, A. Madalan, K. Rissanen, L. Russo, G. Vaughan and J.-M Lehn, *Eur. J. Inorg. Chem.*, 2007, 2944–2965.
90 S. T. Onions, A. M. Frankin, P. N. Horton, M. B. Hursthouse and C. J. Matthews, *Chem. Commun.*, 2003, 2864–2865.
91 W. A. Gobeze, V. A. Milway, B. Moubaraki, K. S. Murray and S. Brooker, *Dalton Trans.*, 2012, **41**, 9708–9721.
92 Y.-T. Wang, S.-T. Li, S.-Q. Wu, A.-L. Cui, D.-Z. Shen and H.-Z. Kou, *J. Am. Chem. Soc.*, 2013, **135**, 5942–5945.
93 S.-Q. Wu, Y.-T. Wang, A.-L. Cui and H.-Z. Kou, *Inorg. Chem.*, 2014, **53**, 2613–2618.
94 S. Dhers, A. Mondal, D. Aguilà, J. Ramírez, S. Vela, P. Dechambenoit, M. Rouzières, J. R. Nitschke, R. Clérac and J.-M. Lehn, *J. Am. Chem. Soc.*, 2018, **140**, 8218–8227.
95 A. Lakma, R. N. Pradhan, S. M. Hossain, J. van Leusen, P. Kögerler and A. K. Singh, *Inorg. Chim. Acta*, 2019, **486**, 88–94.
96 B. Warżajtis, B. Đ. Glišić, N. S. Radulović, U. Rychlewska and M. I. Djuran, *Polyhedron*, 2014, **79**, 221–228.
97 D. P. Ašanin, M. D. Živković, S. Rajković, B. Warżajtis, U. Rychlewska and M. I. Djuran, *Polyhedron*, 2013, **51**, 255–262.
98 A. M. Stadler, F. Puntoriero, F. Nastasi, S. Campagna and J. M. Lehn, *Chem.–Eur. J.*, 2010, **16**, 5645–5660.
99 J. Ramirez, A.-M. Stadler, G. Rogez, M. Drillon and J.-M. Lehn, *Inorg. Chem.*, 2009, **48**, 2456–2463.

100 R. W. Hogue, S. Dhers, R. M. Hellyer, J. Luo, G. S. Hanan, D. S. Larsen, A. L. Garden and S. Brooker, *Chem.–Eur. J.*, 2017, **23**, 14193–14199.
101 J. Hausmann and S. Brooker, *Chem. Commun.*, 2004, 1530–1531, DOI: 10.1039/B403905J.
102 J. Hausmann and S. Brooker, *Chem. Commun.*, 2004, 1530–1531.
103 J. Hausmann, G. B. Jameson and S. Brooker, *Chem. Commun.*, 2003, 2992–2993.
104 J. Klingele, J. F. Boas, J. R. Pilbrow, B. Moubaraki, K. S. Murray, K. J. Berry, K. A. Hunter, G. B. Jameson, P. D. Boyd and S. Brooker, *Dalton Trans.*, 2007, 633–645.
105 N. C. Desai, A. H. Makwana and R. D. Senta, *J. Saudi Chem. Soc.*, 2016, **20**, 686–694.
106 N. Desai, A. H. Makwana and R. Senta, *J. Saudi Chem. Soc.*, 2016, **20**, 686–694.
107 R. Shanmugakala, P. Tharmaraj, C. D. Sheela and C. Anitha, *Int. J. Inorg. Chem.*, 2012, **2012**, 301086.
108 N. S. Mewada, D. R. Shah, H. P. Lakum and K. H. Chikhalia, *J. Assoc. Arab Univ. Basic Appl. Sci.*, 2016, **20**, 8–18.
109 J. Ramírez, A.-M. Stadler, N. Kyritsakas and J.-M. Lehn, *Chem. Commun.*, 2007, 237–239, DOI: 10.1039/B612222A.
110 P. de Hoog, P. Gamez, W. L. Driessen and J. Reedijk, *Tetrahedron Lett.*, 2002, **43**, 6783–6786.
111 A. Das, S. Demeshko, S. Dechert and F. Meyer, *Eur. J. Inorg. Chem.*, 2011, 1240–1248.
112 N. Parizel, J. Ramírez, C. Burg, S. Choua, M. Bernard, S. Gambarelli, V. Maurel, L. Brelot, J.-M. Lehn, P. Turek and A.-M. Stadler, *Chem. Commun.*, 2011, **47**, 10951–10953.
113 M. Quesada, M. Monrabal, G. Aromí, V. A. de la Peña-O'Shea, M. Gich, E. Molins, O. Roubeau, S. J. Teat, E. J. MacLean, P. Gamez and J. Reedijk, *J. Mater. Chem.*, 2006, **16**, 2669–2676.
114 J. S. Costa, K. Lappalainen, G. de Ruiter, M. Quesada, J. Tang, I. Mutikainen, U. Turpeinen, C. M. Grunert, P. Gütlich, H. Z. Lazar, J.-F. Létard, P. Gamez and J. Reedijk, *Inorg. Chem.*, 2007, **46**, 4079–4089.
115 S. Bonnet, M. A. Siegler, J. S. Costa, G. Molnár, A. Bousseksou, A. L. Spek, P. Gamez and J. Reedijk, *Chem. Commun.*, 2008, 5619–5621, DOI: 10.1039/B811746B.
116 S. Bonnet, G. Molnár, J. Sanchez Costa, M. A. Siegler, A. L. Spek, A. Bousseksou, W.-T. Fu, P. Gamez and J. Reedijk, *Chem. Mater.*, 2009, **21**, 1123–1136.
117 M. Quesada, V. A. de la Peña-O'Shea, G. Aromí, S. Geremia, C. Massera, O. Roubeau, P. Gamez and J. Reedijk, *Adv. Mater.*, 2007, **19**, 1397–1402.
118 T. M. Ross, B. Moubaraki, S. M. Neville, S. R. Batten and K. S. Murray, *Dalton Trans.*, 2012, **41**, 1512–1523.
119 T. M. Ross, B. Moubaraki, S. R. Batten and K. S. Murray, *Dalton Trans.*, 2012, **41**, 2571–2581.
120 T. M. Ross, B. Moubaraki, K. S. Wallwork, S. R. Batten and K. S. Murray, *Dalton Trans.*, 2011, **40**, 10147–10155.
121 T. M. Ross, B. Moubaraki, D. R. Turner, G. J. Halder, G. Chastanet, S. M. Neville, J. D. Cashion, J.-F. Létard, S. R. Batten and K. S. Murray, *Eur. J. Inorg. Chem.*, 2011, 1395–1417.
122 N. Wannarit, N. Nassirinia, S. Amani, N. Masciocchi, S. Youngme, O. Roubeau, S. J. Teat and P. Gamez, *Inorg. Chem.*, 2014, **53**, 9827–9836.
123 J. Lu, Y.-Q. Zhang, X.-L. Li, M. Guo, J. Wu, L. Zhao and J. Tang, *Inorg. Chem.*, 2019, **58**, 5715–5724.
124 H. T. Chifotides and K. R. Dunbar, *Acc. Chem. Res.*, 2013, **46**, 894–906.
125 M. Savastano, C. Bazzicalupi, C. Giorgi, C. García-Gallarín, M. D. López de la Torre, F. Pichierri, A. Bianchi and M. Melguizo, *Inorg. Chem.*, 2016, **55**, 8013–8024.
126 M. Savastano, C. Bazzicalupi, C. García, C. Gellini, M. D. López de la Torre, P. Mariani, F. Pichierri, A. Bianchi and M. Melguizo, *Dalton Trans.*, 2017, **46**, 4518–4529.
127 M. Savastano, C. García-Gallarín, M. D. López de la Torre, C. Bazzicalupi, A. Bianchi and M. Melguizo, *Coord. Chem. Rev.*, 2019, **397**, 112–137.
128 B. J. Jordan, M. A. Pollier, L. A. Miller, C. Tiernan, G. Clavier, P. Audebert and V. M. Rotello, *Org. Lett.*, 2007, **9**, 2835–2838.
129 Q. Zhou, P. Audebert, G. Clavier, R. Méallet-Renault, F. Miomandre, Z. Shaukat, T.-T. Vu and J. Tang, *J. Phys. Chem. C*, 2011, **115**, 21899–21906.
130 E. Kurach, D. Djurado, J. Rimarčik, A. Kornet, M. Wlostowski, V. Lukeš, J. Pécaut, M. Zagorska and A. Pron, *Phys. Chem. Chem. Phys.*, 2011, **13**, 2690–2700.
131 G. Clavier and P. Audebert, *Chem. Rev.*, 2010, **110**, 3299–3314.
132 J. Li, Y. Peng, H. Liang, Y. Yu, B. Xin, G. Li, Z. Shi and S. Feng, *Eur. J. Inorg. Chem.*, 2011, 2712–2719.
133 O. Stetsiuk, A. Abhervé and N. Avarvari, *Dalton Trans.*, 2020, **49**, 5759–5777.
134 B. S. Dolinar, S. Gómez-Coca, D. I. Alexandropoulos and K. R. Dunbar, *Chem. Commun.*, 2017, **53**, 2283–2286.
135 D. I. Alexandropoulos, B. S. Dolinar, K. R. Vignesh and K. R. Dunbar, *J. Am. Chem. Soc.*, 2017, **139**, 11040–11043.
136 T. Lacelle, G. Brunet, A. Pialat, R. J. Holmberg, Y. Lan, B. Gabidullin, I. Korobkov, W. Wernsdorfer and M. Murugesu, *Dalton Trans.*, 2017, **46**, 2471–2478.
137 M. A. Lemes, G. Brunet, A. Pialat, L. Ungur, I. Korobkov and M. Murugesu, *Chem. Commun.*, 2017, **53**, 8660–8663.
138 D. Luneau, F. M. Romero and R. Ziessel, *Inorg. Chem.*, 1998, **37**, 5078–5087.
139 T. M. Barclay, R. G. Hicks, M. T. Lemaire and L. K. Thompson, *Inorg. Chem.*, 2001, **40**, 5581–5584.
140 M. A. Lemes, N. Mavragani, P. Richardson, Y. Zhang, B. Gabidullin, J. L. Brusso, J. O. Moilanen and M. Murugesu, *Inorg. Chem. Front.*, 2020, **7**, 2592–2601.